

Physical Processes and Applications of the Monte Carlo Radiative Energy Deposition (MRED) Code

Robert A. Reed, *Fellow, IEEE*, Robert A. Weller, *Senior Member, IEEE*, Marcus H. Mendenhall, Daniel M. Fleetwood, *Fellow, IEEE*, Kevin M. Warren, Brian D. Sierawski, *Senior Member, IEEE*, Michael P. King, *Member, IEEE*, Ronald D. Schrimpf, *Fellow, IEEE*, and Elizabeth C. Auden, *Member, IEEE*

Abstract—MRED is a Python-language scriptable computer application that simulates radiation transport. It is the computational engine for the on-line tool CRÈME-MC. MRED is based on c++ code from Geant4 with additional Fortran components to simulate electron transport and nuclear reactions with high precision. We provide a detailed description of the structure of MRED and the implementation of the simulation of physical processes used to simulate radiation effects in electronic devices and circuits. Extensive discussion and references are provided that illustrate the validation of models used to implement specific simulations of relevant physical processes. Several applications of MRED are summarized that demonstrate its ability to predict and describe basic physical phenomena associated with irradiation of electronic circuits and devices. These include effects from single particle radiation (including both direct ionization and indirect ionization effects), dose enhancement effects, and displacement damage effects. MRED simulations have also helped to identify new single event upset mechanisms not previously observed by experiment, but since confirmed, including upsets due to muons and energetic electrons.

Index Terms—Displacement damage, Monte Carlo, MRED, radiation effects, radiation transport, single event effects, single event upset, total ionizing dose.

I. INTRODUCTION

THE Monte Carlo method for radiation transport has proven to be a useful, and often necessary, tool to evaluate the basic mechanisms associated with radiation-induced failures in electronics. As of today, more than 250 research papers have been published on this topic by more than 16 organizations [1], [2]. This article is the third in a series of review papers on the development and application of Vanderbilt University's computer code Monte Carlo Radiative Energy Deposition (MRED). The first paper [3] defined how MRED is used to

Manuscript received March 05, 2015; revised June 23, 2015; accepted June 28, 2015. Date of publication August 10, 2015; date of current version August 14, 2015. This work was supported by NASA, the DTRA Basic Research Program, the DTRA Radiation Hardened Microelectronics Program, and internal funds from Vanderbilt University.

R. A. Reed, R. A. Weller, D. M. Fleetwood, K. M. Warren, B. D. Sierawski, and R. D. Schrimpf are with the Department of Electrical Engineering and Computer Science, Vanderbilt University, Nashville, TN 37215 USA (e-mail: robert.reed@vanderbilt.edu).

M. H. Mendenhall is with National Institute for Standards and Technology, Gaithersburg, MD 20899 USA.

M. P. King and E. C. Auden are with Sandia National Laboratories, Albuquerque, NM 87123 USA.

Color versions of one or more of the figures in this paper are available online at <http://ieeexplore.ieee.org>.

Digital Object Identifier 10.1109/TNS.2015.2454446

compute single event upset rates. The second paper [1], [2] provides an anthology of the development of radiation transport tools intended to study single event effects; the history of the development of MRED is included. This paper provides a detailed summary of the physical processes included in MRED, and a selected set of applications.

The MRED code integrates the physics processes associated with the Geant4 toolkit [4]–[6] with Fortran codes PENELOPE 2008, an electron transport code, and CEM03 and LAQGSM [7]–[9], both nuclear physics codes. This integration brings together accurate and well-tested physics codes to address key issues associated with radiation effects in electronics. This review paper begins with a detailed discussion of the physical processes enabled within MRED. This is followed by an overview of how MRED has been used to investigate the basic mechanisms for single event upset (SEU), displacement damage, and total ionizing dose (TID) effects. SEUs produced by heavy ion nuclear reactions in hardened static random-access memories (SRAMs) are discussed in Section III. Sections IV–VI describe SEUs produced by a single proton, muon, or electron. Section VII describes multiple bit upsets. Section VIII describes dose enhancement effects due to high-Z materials near oxides. And finally, Section IX discusses displacement damage. These results indicate the breadth of applications to which MRED has been applied, and illustrate the versatility of Monte Carlo transport codes in assisting in a broad range of radiation effects simulation and analysis.

II. MRED

This section is the definitive reference for the physics simulated in MRED 9.6, which is presently intended to be the final version of MRED, and the one used by CRÈME-MC. In this regard, we note that the CRÈME web site was updated in January 2015 to include updates of the MRED and Geant4 versions in use. At that time the Geant4 version used to build MRED was frozen at 9.6. In the interest of stability, all feature updates to MRED were also terminated.

MRED is a radiation transport code, which serves as the core computation engine for CREME-MC [3].¹ It is based on Geant4, which is a product of a worldwide collaboration to support high-energy physics detector simulation [4]–[6]. The name Geant4 derives from “geometry and tracking,” which is a concise summary of what the code does. The user must tailor a Geant4 application to a specific purpose. Geant4 was originally undertaken

¹MRED was designed and written by R. A. Weller and M. H. Mendenhall.

as a rewrite in the c++ language of earlier software, Geant3, which itself was the product of decades of development in support of particle and nuclear physics.

Geant4 is not a monolithic computer program but rather a collection of c++ class libraries that implement virtual device creation, particle tracking, and the physical processes through which radiation interacts with matter. The ordinary paradigm is that these classes are assembled into a full, executable c++ program by using the geometry classes to build a virtual model of a detector or other structure, and using the physics and tracking classes to simulate the effects of radiation on the structure. The relevant results of such a simulation are particular to the problem at hand. In this sense, each Geant4 application represents a unique framework in which to test, improve, and validate the core components of the system. This is particularly so with the physics classes that describe the interaction of radiation with matter. MRED is a Python language program that includes Geant4 classes and additional Fortran language components for computing energy deposition in semiconductor-device size structures.

MRED presently exists in three slightly different forms: (1) the complete one described in this paper that is used for all Vanderbilt publications, (2) the CREME-MC form, which omits Fortran Penelope 2008, and (3) an older form created to facilitate collaboration between ourselves and others called VRT, which was forked on 16-Mar-2011, and which omits all Fortran additions and subsequent modifications of the core code, except for a small number of bug fixes.

MRED computes energy deposition in semiconductor-device size structures. By assuming the well known relationship between deposited energy and average rate of generated charge in silicon, 3.6 eV per electron-hole (e-h) pair [10], the excess charge produced by radiation in devices is approximated. MRED has many other capabilities, including differentiating energy going into atomic motion (displacement damage) and electronic excitation (charge generation), but simulating deposited energy is its principal function. As a result, the central objective of MRED is to compute this quantity as accurately and precisely as current knowledge permits. Since displacement damage is frequently important for ion and neutron irradiation of semiconductors, MRED also tracks separately the energy transferred to atoms of the medium by atomic collisions in solids. This quantity is related to lattice defect production and can be used to estimate displacement damage effects. However, as of this writing, the association of energy deposited in atomic motion in a device with specific *electrically active* defects or the number thereof has not been established quantitatively.

To achieve the necessary flexibility and extensibility for MRED, we implemented the simulation in Python [11], [12]. MRED is implemented as a collection of related modules containing Python classes, which in many cases are quite close analogs of underlying Geant4 c++ classes, and in others are unique and highly specialized. MRED incorporates c++ and Fortran core computing components into a Python environment using an automatic c++ code generator called SWIG, the Simplified Wrapper Interface Generator [13]–[15], which creates satisfactory interfaces in Python to a very large number of underlying c++ (and Fortran through c++) objects with min-

imal programming effort. This is a key point, since reducing the amount of code that must be written by hand reduces the likelihood of errors.

While MRED contains many lines of custom code written in Python, c++, and Fortran, the underlying physics and geometry code is all written by subject-matter experts in the Geant4 collaboration. This code is externally documented, frequently with extensive validation. While no software can be assumed to be free of error, restricting key components of MRED to code designed, implemented, and maintained openly by the scientific community is the most effective quality control strategy available, and the only one suitable for a reference computation such as CRÈME-MC is designed to produce.

The theory, general structure, and operation of MRED have been described previously [3]. In the paragraphs that follow, we describe explicitly at the level of Geant4 classes the relevant physics used by MRED and the subset used to implement CRÈME-MC. This description is accompanied by references to the literature or sources, which describe the computations and/or algorithms used. We have not undertaken to duplicate the comparisons with experimental data or other calculations that have been used for quality control by the original authors of the components used to build MRED, but we have in many cases compared MRED output with experimental data to help inform decisions on how to bring together the various independent and alternative physical process descriptions to realize the form of MRED that is used by CRÈME-MC.

The central role of energy deposition through electronic processes mandates that the most detailed description of electromagnetic processes available be used in microelectronic device simulations. To achieve this, MRED uses a variant of the *G4EmStandardPhysics_option4²* class, which is the most detailed of all of the electromagnetic physics classes in Geant4. The name of the corresponding MRED class is *VUPhysListEmStandardScreened*. It differs primarily in its use of *G4ScreenedNuclearRecoil* to describe multiple scattering and Coulomb scattering of nuclei in solids [16].

The energy deposited in atomic motion, i.e., non-ionizing energy loss, is computed by accumulating the endpoint energies of ions generated by the Geant4 class *G4ScreenedNuclearRecoil* in specific user-defined sensitive volumes in a device [17]. Note that MRED does not use a parameterization of nuclear stopping power. Nuclear stopping power is simply the accumulated average of energy deposited in ion-ion atomic collisions in solids. MRED computes these collisions explicitly and generates trackable recoil ions with energies as low as approximately 5 keV. Collisions that transfer less energy than this to a target atom result in the deposition of energy but no trackable secondary particles. Energy transfers down to several tens of eV are computed. The cumulative results of a large number of such energy transfers create the observed non-ionizing energy loss and multiple scattering, the latter of which agrees with analytical multiple scattering theory and experiment [17].

Particles penetrating matter also lose energy through collisions with electrons, although the process cannot be treated in the same way as atomic collisions in solids because of the large

²The names of c++ classes in Geant4 and MRED are indicated in italics.

number of collisions that result in the transfer of small amounts of energy. In [18] the International Commission on Radiation Units identifies five energy loss mechanisms for charged particles. Of these five processes, two are important for radiation effects in electronics. The first occurs when the incident ion produces electronic excitation and ionization of the target. The average energy lost by a projectile per unit of trajectory from ionization is called electronic stopping power. The second occurs when the incident ion produces recoiling target nuclei (called recoil loss in [18]). The average energy lost by a projectile per unit of trajectory from recoils is called nuclear stopping power.

Formally, the average energy lost per unit of trajectory, or linear energy transfer (LET), is the average of all stopping processes defined in [18]; the components of LET that are of interest for electronics are the sums of electronic stopping and nuclear stopping. Electronic stopping tends to dominate for most ions in the space environment. For this reason, the radiation effects community typically associates the metric LET with electronic stopping, ignoring the contribution from all other stopping processes.

In a binary collision Monte Carlo simulation, electronic stopping must be partitioned into one component that is considered to be a constant force along the trajectory slowing the projectile, and a second that is energy lost in the production of discrete, trackable electrons, or as they are commonly called, δ -rays. The partitioning must occur in such a way that the average of energy lost to discrete trackable electrons and the energy lost along the trajectory sum to the total LET. This process clearly has a strong influence on the complexity of the simulation, since a large number of low energy δ -rays can take a very large amount of computer time to track. Geant4 handles this and the process of δ -ray production by photons through a parameter called the production cut. Although production cuts are actually expressed in length units for technical reasons beyond the scope of this review, one may think of production cuts as the threshold energy for producing discrete trackable particles. The details of this process are in the Geant4 Physics Reference Manual [6].

Additional Geant4 processes are available in MRED when used independently of CRÈME-MC; many of these were used for the computations described in papers cited elsewhere in this review. Some, such as the process to describe the interaction of gamma rays with nuclei contained in *G4EmExtraPhysics*, are part of the standard Geant4 release. Others are custom. For example, MRED incorporates the high precision electron and positron transport code PENELOPE 2008 [19]–[24].³ Although Geant4 includes a subset of the Fortran PENELOPE 2008 physics models (ionization, bremsstrahlung, etc.) rewritten in the c++ language, it does not use Penelope 2008's multiple scattering model. The effect of this is most apparent on the trajectories of low energy electrons in small volumes, where Fortran PENELOPE 2008 tracks are substantially more physical in appearance than those produced by the native Geant4 version.

The Fortran PENELOPE 2008 is implemented in MRED using a class *VUPhysListEmPenelopeQED*. A c++ implemen-

tation of PENELOPE, *G4PenelopeIonisationModel*, is also available as part of the standard Geant4 release and is used in both *VUPhysListEmPenelopeQED* and *VUPhysListEmStandardScreened*. However, in *VUPhysListEmPenelopeQED* the user has the option of using the Fortran version for transport of electrons, positrons, and photons below an adjustable threshold, which is nominally set at 50 keV. For detailed information about PENELOPE 2008, readers are referred to [21] and references therein. Additional details on the electromagnetic physics in *VUPhysListEmPenelopeQED* and *VUPhysListEmStandardScreened* can be obtained from an analysis of the available source code of *G4EmStandardPhysics_option4*, from which both were derived, and [6], which also contains a significant amount of material on validation of all aspects of Geant4 physics.

When MRED was under development, the role of nuclear reactions induced by heavy ions in single event effects was not widely appreciated by the radiation effects community. Indeed, as reviewed previously [3], the introduction of MRED was instrumental in revealing many such effects. Since CRÈME96 only treats stopping power by ions and not nuclear reactions, the presence of these effects was one of the strong motivations for the creation of CRÈME-MC. Unfortunately, the classes available in Geant4 for simulating these nuclear reactions were not comprehensive, either in their coverage of various primary ions or in applicability to the full range of energies of typical cosmic rays relevant to single event effects in spacecraft. As a result, MRED has highly advanced Fortran extensions for treating nuclear reactions that were developed by researchers at Los Alamos National Laboratory [7].

The programs used to describe nuclear reactions in MRED are called CEM03 and LAQGSM. These are used for protons (CEM03) and all nuclear projectiles heavier than protons (LAQGSM) [7]. The CEM03 and LAQGSM codes have been extensively tested and validated by their authors [7]–[9]. The integration of CEM03 (3.03) is achieved by replacing the Bertini cascade code in the standard Geant4 physics list *HadronPhysicsFTFP_BERT_HP* with the Fortran CEM03 computation, made accessible to Geant4 through a custom c++ interface class *VUCEMProtonBuilder*. The MRED class is called *HadronPhysicsFTFP_CEM_HP*. Because of namespace issues, some modifications of the Fortran of CEM03 and LAQGSM are necessary. These are accomplished automatically by a preprocessing step (by a Python script) prior to compilation. CEM03 is used to describe proton-induced nuclear reactions for energies up to 5 GeV. Above 5 GeV *HadronPhysicsFTFP_CEM_HP* is identical to *HadronPhysicsFTFP_BERT_HP* (see the Geant4 source code and [6] for details).

Nuclear reactions induced by helium and all heavier nuclei are computed in MRED by the class *PhysListIonInelasticLAQGSM*, which uses the (pre-processed) Fortran LAQGSM 3.03 code through a c++ interface, for all projectile energies. These two programs provide comprehensive nuclear-reaction final-state computations for reactions relevant to semiconductors with one possible exception. For technical reasons, protons in the target are ignored. It is unlikely that this omission is relevant to any practical situations, but in the event that consid-

³The Fortran code, PENELOPE 2008, and a custom interface linking it with Geant4 have been made available to us by PENELOPE's author, F. Salvat, and through collaboration with M. Asai, Stanford Linear Accelerator Center, Stanford University.

eration of such reactions is indicated, standard Geant4 nuclear reaction classes must be used. These are available in MRED but are not accessible via CRÈME-MC.

Nuclear reactions caused by neutrons are also computed by *HadronPhysicsFTFP_CEM_HP*. CEM03 is used for neutrons with energies from 20 MeV to 5 GeV. Below 20 MeV, neutron interactions are described by code in the Geant4 class *G4NeutronHPBuilder*, which is based on extensive measured numerical data, as opposed to theory. *HadronPhysicsFTFP_CEM_HP* is also used to describe the hadronic interactions of pions and kaons. However, the hadronic interactions of all other elementary particles are handled in *HadronPhysicsFTFP_CEM_HP* exactly as they are in the standard Geant4 physics list *HadronPhysicsFTFP_BERT_HP*. Elementary-particle and radioactive decay are described in an MRED class *PhysListDecay*, which is essentially a merged version of the two distinct Geant4 classes *G4DecayPhysics* and *G4RadioactiveDecayPhysics*. Finally, elastic hadron collisions are described by the standard Geant4 class *G4HadronElasticPhysicsHP*.

Importantly, MRED uses a variance reduction strategy when computing the effects of nuclear reactions [3]. Although nuclear reactions induced by cosmic rays are quite rare in comparison with simple ion strikes, their impacts on the production of single event effects are large. Indeed, in many circumstances virtually all single event effects are a consequence of nuclear reactions. As a result, in the absence of variance reduction, the uncertainty can be very large. MRED deals with this by artificially boosting the cross section for nuclear reactions by a user-selectable factor of up to several thousand. This produces many more nuclear reactions than are physically correct, but this error is addressed by reducing the statistical weight of events that include nuclear reactions to precisely compensate. This scheme and other aspects of variance reduction were originally discussed in [3]. Since the publication of that paper, the cross section weighting scheme has been improved, placed on firm theoretical ground, and extensively tested for validity [25]. CRÈME-MC uses the new algorithm.

MRED has been under continuous version control using subversion since March, 2005, and was under version control with centralized version control (CVS) from the very beginning until the CVS-to-subversion transition, and successive production versions were tested for consistency. Generally speaking, changes in Geant4 relevant to MRED have been relatively modest from version to version. Because we use LAQGSM and CEM03 for nuclear physics calculations, and our own ion-solid collision code for multiple scattering events, we have been further isolated since approximately 2010 from Geant4 evolution. MRED has been frozen both in its features and in the Geant4 version since roughly the time that Geant4 9.6 was released. Currently there are no plans for either additional features or for tracking Geant4 changes other than patches to Geant4 9.6.

CRÈME is designed to produce reference computations. As a result, updating the system is infrequent and undertaken with great care to minimize the likelihood of regression errors. The 2015 update of the CRÈME web site involved significant modifications, the first in several years, including updates of both the MRED and Geant4 versions in use. At the time of this writing,

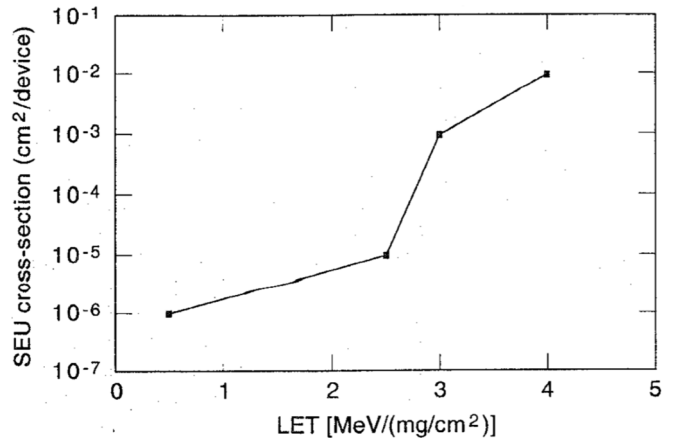


Fig. 1. Calculations by Koga, et al. [29] of the SEU cross section curve including nuclear reactions. The 0.5 MeV cm²/mg SEU cross section is a prediction based on the nuclear cross section of 200 MeV carbon on silicon.

Geant4 version 9.6 was at Patch-03, and it is unlikely, although not impossible, that another patch will be forthcoming from the Geant4 collaboration. The full source of Geant4 9.6 Patch-03 can be obtained from the Geant4 web site at CERN [6].

The following sections provide a more general overview of a variety of MRED applications that are designed to address radiation effects in electronic circuits and devices. In each case, MRED has enabled new insight into basic radiation effects mechanisms, and/or enabled a more accurate prediction of error rates for devices and ICs in space applications.

III. MODELING OF HEAVY ION NUCLEAR REACTION-INDUCED SEUS IN HARDEN SRAMS

High-energy protons and high-energy heavy ions ($Z > 1$) can interact with the nuclei of the materials. This can result in displacement or fragmentation of the nuclei into charged ionizing species that can propagate to sensitive regions within a semiconductor device [26], [27]. The effects of nuclear reactions from heavy ions have only begun to be considered recently. For example, Ecoffet, *et al.*, proposed in 1997 that ion-nuclear reactions could play a role in SEU cross section measurements [28]. They presented data and analysis that suggested that up to 10% of the events observed for interactions of high-energy carbon beams with SRAMs and DRAMs with low SEU cross sections could be attributed to nuclear reactions. The issue was revisited in 1998 by Koga, *et al.*, who analyzed SEU results obtained by exposing their components to relativistic heavy ions [29]. They maintained that small (relative to the saturation cross section) SEU cross sections should be observed in the low linear energy transfer (LET), ~ 1 MeV cm²/mg, region when the primary ion species is sufficiently energetic. Furthermore, they suggested that in this region the cross section would be largely independent of the LET of the primary ion, as illustrated in Fig. 1.

In Warren, *et al.* [30], a second plateau effect at low LET was observed in heavy ion SEU cross section measurements for a hardened SRAM (Fig. 2). Here the data show a plateau over a much broader range of LET (~ 1 to ~ 40 MeV cm²/mg), in addition to the usual saturation plateau. Circuit and device level

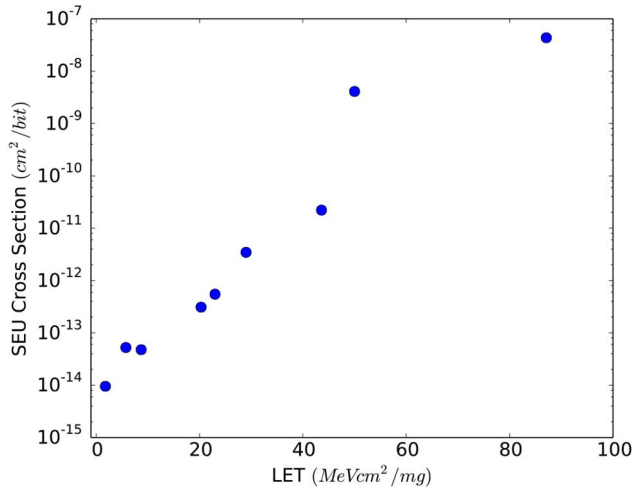


Fig. 2. Heavy ion data taken from Warren, et al. [30] showing a low-LET tail in addition to the typical SEU saturation cross section.

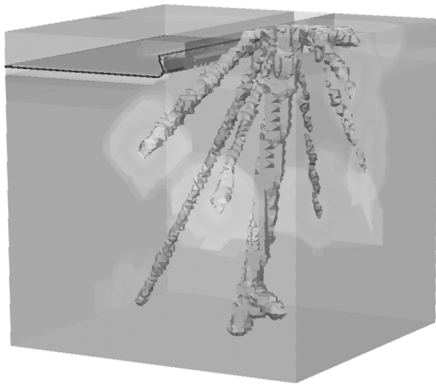


Fig. 3. MRED (V6G4.7.0)⁴ simulation of secondary ion shower produced from the interaction of 523 MeV neon with a tungsten nuclei located in the interconnect layer of a CMOS process. (After [26]).

analyses indicated a critical charge and sensitive volume structure that could not be reconciled with the observed SEU rate below 40 MeV cm²/mg unless nuclear reactions were considered in the SEU analysis and error rate calculations. As we now show, MRED modeling and simulation enables a more accurate prediction of error rates for these devices than conventional methods that do not include a full range of nuclear interactions.

1) *Basic Modeling Considerations:* Interactions of high-energy ions with the nuclei of the materials that make up integrated circuits (e.g., silicon, aluminum, copper, tungsten) that result in the production of secondary ions from fragmentation or displacement are rare with respect to ion-electron interactions that collectively lead to the observed electronic stopping power. However, when nuclear reactions occur, they produce one or more secondary ionizing particles with substantially different LET than the incident particle. Fig. 3 contains an example of the secondary ion shower resulting from the interaction of a 523 MeV neon ion with a tungsten nucleus.

Simulation of the effects of nuclear reactions on single event cross sections are demonstrated in Fig. 4. Electronic stopping dominates the energy loss process for most of the primary ions.

⁴Version 6 of MRED and version G4.7.0 were used to generate this image. This notation is used throughout this paper to identify the MRED and Geant4 versions used for each simulation result.

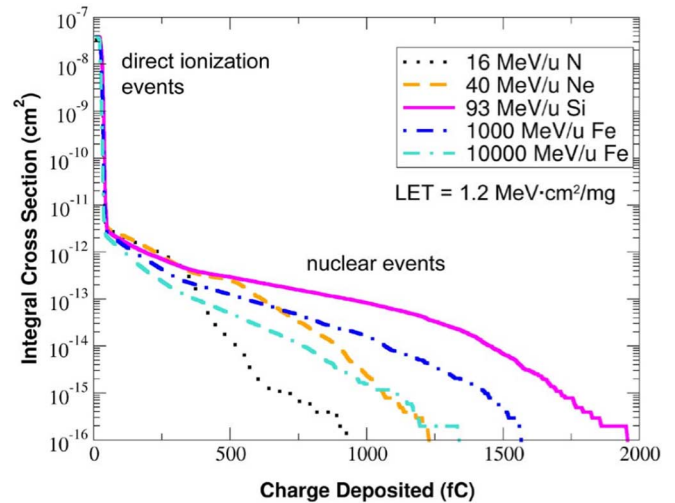


Fig. 4. The cumulative statistical distribution of measured events as a function of charge deposited in a sensitive volume for a series of ions (after [31]). The most probable events are those associated with charge generation at the LET peak, which is approximately 100 fC. Higher charge events can be seen when nuclear reactions are included that extend approximately an order of magnitude beyond that associated with a traditional stopping power calculation.

This process generates approximately 100 fC of charge in the $4 \mu\text{m}^2 \times 2.25 \mu\text{m}$ sensitive volume. However, rare nuclear reactions can lead to charge generation within the sensitive volume that exceeds the LET peak by over an order of magnitude. The ions in Fig. 4 have roughly the same LET, despite being different species with significantly different energies. Fig. 4 highlights both the relative rarity and significance of nuclear reactions to the integral cross section for a device. If the device in question is sensitive to less than 100 fC of charge, then for this set of ions, SEU from nuclear reactions will be insignificant, as direct ionization events, vastly more numerous, will dominate the response. However, if the device has a critical charge of greater than 500 fC, then the SEU response will be entirely determined by nuclear reactions, because they can deposit so much charge directly within the critical sensitive volume of the device. Without including nuclear processes in the analysis, the predicted SEU rate would be zero. Hence, whether nuclear reactions are significant for error rate calculations is a strong function of the critical charge of the circuit or device of interest. As noted above, because of the rarity of nuclear reactions, MRED uses a variance reduction strategy when computing the effects of nuclear reactions [3], [25] in order to decrease the computation time.

2) *Assistance in Guiding Ground-Based Measurements:* Since the probability of ion-nuclear reactions is small, experimentally determining when they contribute more to the rate than direct ionization can be difficult. Under ideal circumstances one would always employ a rate prediction method that included the necessary physics. However, at the time of this writing such an analysis is not always practical or cost effective. Being able to recognize when nuclear reactions are a potential issue for rate prediction can help reduce the time and expense required to produce a sufficiently accurate error rate estimate.

Inspection of the heavy ion cross-section curve is a useful first step to determine whether nuclear reactions are necessary to consider in error rate calculations. Fig. 5 shows a typical

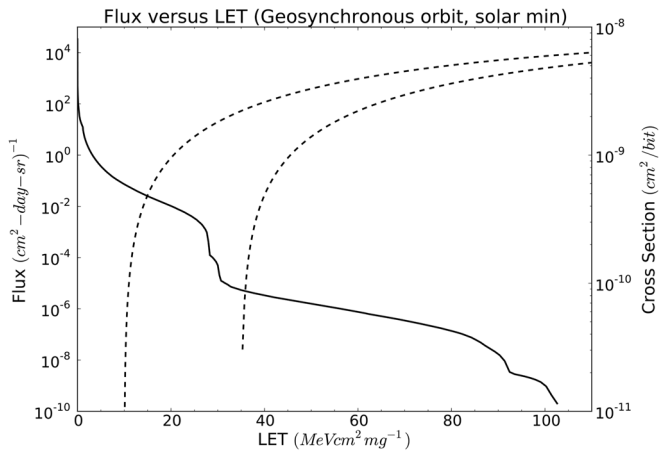


Fig. 5. Heinrich [32] and two hypothetical Weibull curves. The left Weibull curve has a threshold LET of 10 MeVcm²/mg and the right curve has a threshold LET of 35 MeVcm²/mg.

Heinrich curve for a geosynchronous earth orbit environment with two generic Weibull curves. The curve on the left has a threshold of 10 MeV cm²/mg, and the curve on the right has a threshold of 35 MeV cm²/mg. The relative abundance of particles exceeding the threshold for upset for the curve on the left exceeds that of the curve on the right by 3.5 to 4 orders of magnitude. Hence, the Weibull curve on the left is more likely to be dominated by direct ionization events, whereas the curve on the right is more likely to be influenced or even dominated by nuclear reactions.

The case of ions having the same LET but different mass and energy also typically indicates that more advanced modeling (beyond direct ionization alone) is warranted. For example, Fig. 6 contains heavy ion broad beam SEU data for a hardened 128 K SRAM [33] from two different ground-based facilities: The Texas A&M Cyclotron Facility and the Brookhaven National Laboratory's Tandem Van de Graaff facility. The former accelerator has the capability to produce particles with larger energy per nucleon than the latter. From the figure it is readily apparent that the measured SEU cross section depends on ion energy. While it is impossible to formally prove that the difference is due to nuclear reactions (whose probability and secondary ion profile depends on energy), it is consistent with MRED model results on a hardened SRAM [30]. Hence, for environments and devices that likely are sensitive to nuclear reaction events, facilities that enable the use of higher-energy ions will enable more accurate estimates of error rates.

3) *Impact on SEU Rate Calculations:* The first definitively observed effect of nuclear reactions on in-flight SEU rates was for a hardened SRAM aboard the MESSENGER mission. A subset of the data for this component is shown above in Fig. 2. The data show both the low LET plateau as well as the relatively high threshold prior to saturation. Howe *et al.* [34] suggested that for some devices with high LET thresholds, the on-orbit SEU rate could be dominated by nuclear reactions. At the time of that work, best practices dictated performing two Weibull fits, one to the smaller SEU cross sections and one to the larger set. Then the two were combined into a single rate calculation via the integral rectangular parallelepiped (IRPP) approach. The

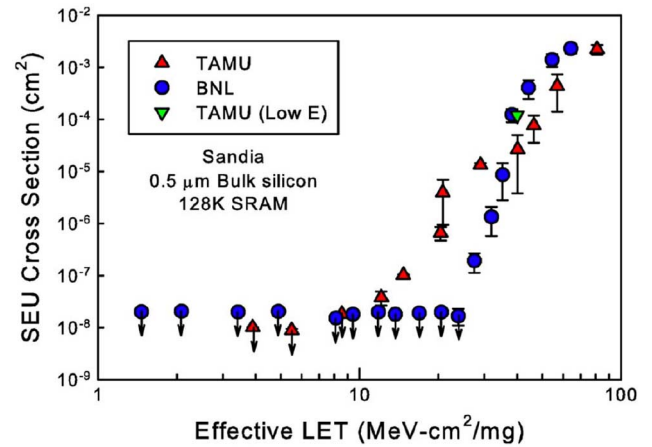


Fig. 6. Heavy ion broad beam data taken on a hardened 128k SRAM. The figure highlights the dependence of the ion energy and not just LET on the measured SEU response. (After [33]).

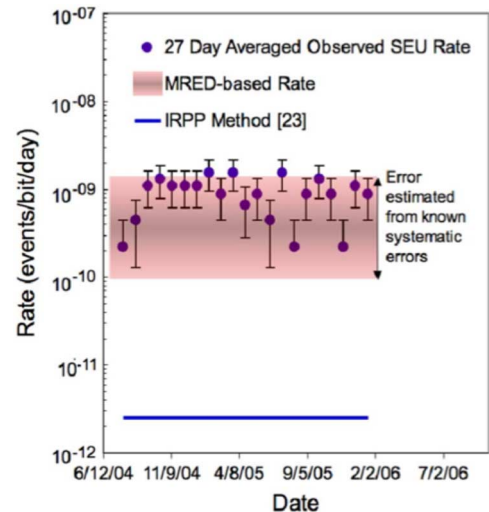


Fig. 7. On-orbit SEU rate for a hardened SRAM relative to MRED (V8 G4.8.1) predictions including nuclear reactions and the traditional IRPP method. (After [35]).

estimated SEU rate for the interplanetary environment was 3×10^{-12} errors/bit-day. The measured rate in flight was between 5×10^{-10} and 10^{-9} errors/bit-day (Fig. 7), which was roughly 2.5 orders of magnitude higher than the expected SEU rate.

In [35] Reed *et al.* expanded the analysis performed by Howe, *et al.* [34], and used MRED to perform an error rate calculation for the hardened SRAM. A single sensitive volume model was used to identify the charge collection region. The critical charge of the circuit was determined by fitting the experimentally measured SEU cross-section curves as a function of both LET and energy to the measured results. The incorporation of the hadronic physics models detailed in Section II allowed for the creation and propagation of nuclear reaction products. The rate was then calculated using the full range of ion species and energies over the interplanetary environment. The result, including systematic errors, was an estimated rate between 10^{-10} and 10^{-9} errors/bit-day, which is in good agreement with the on-orbit SEU rate, as shown in Fig. 7. The authors concluded

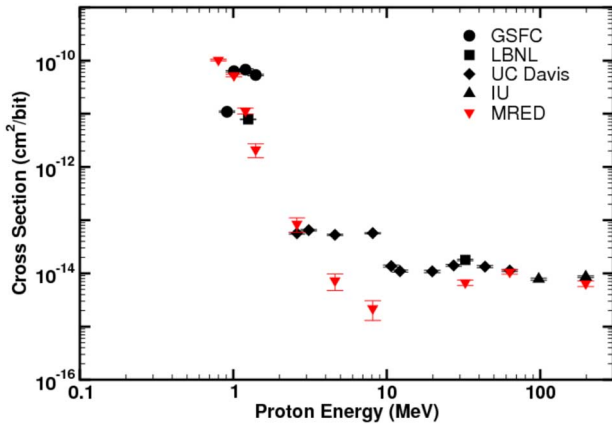


Fig. 8. MRED (V9 G4.9.4) simulation results compared to experimental SEU cross sections. (After [41]).

that error-rate calculations that neglected ion-nuclear interactions were not adequate for modeling the ground-based measurements or accurately predicting the on-orbit error rate. In instances where the relative contribution of nuclear reactions may be comparable to or greater than ionization processes, one must use a more detailed modeling approach, e.g., as enabled in MRED.

IV. MODELING OF PROTON-INDUCED SEUS IN SRAMS

Proton-induced upsets are typically the result of the interaction of an energetic proton with an atom in or near the sensitive volume of a device, leading to the production of a much higher-LET ion than the incident particle via indirect ionization [36], [37]. Early evidence that commercial SRAMs also could be upset by low-energy protons as a result of direct ionization was suggested by experimental results presented at RADECS 2006 by Gerardin *et al.* [38]. A convincing dataset of upsets as a function of the incident angle was subsequently published by Rodbell and co-workers from IBM [39]. This work established that direct ionization due to protons is an upset mechanism that must be considered for space applications using 65 nm technologies and below.

Since the initial publications, proton ionization events have been reported in various technologies, including both bulk and SOI [40]–[47]. For example, Sierawski *et al.* [41] presented SEU test results on a 65 nm bulk CMOS SRAM using proton beams at the Indiana University Cyclotron Facility (IUCF), the University of California Davis Crocker Nuclear Laboratory, and the NASA Goddard Radiation Effects Facility. The experimental data (black symbols) in Fig. 8 show proton-induced SEU cross sections that differ by orders of magnitude between low and high energy [41]. SEU cross sections were collected at normal incidence across a large number of energy tunes and facilities, ruling out conclusively the possibility of experimental artifacts. Combining these types of experiments with MRED modeling results enabled the identification of the dominant proton transport mechanisms that produce SEUs at various energies [41].

1) *Physical Modeling*: A complete picture of the memory response spanning the entire proton energy range can only be

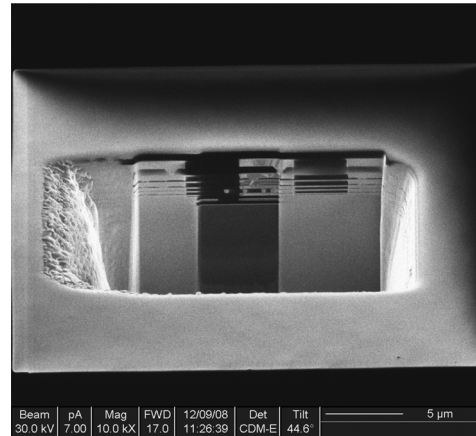


Fig. 9. SRAM material cross section exposed by focused ion beam.

obtained through simulations able to capture the physical processes of proton-induced ionization, Coulomb scattering, and spallation nuclear reactions. To accomplish this, we developed a physical model and calibrated a sensitive volume model to investigate the mechanisms for upset for the 65 nm SRAM in [41]. To facilitate experimental validation, the SRAM was bonded as a chip-on-board to allow low-energy particles to penetrate into the active silicon region without ranging out. Low-energy protons have a range of only a few micrometers and the electronic stopping power rapidly changes as the proton loses energy.

Building a virtual model of the SRAM to demonstrate the upset mechanism of ionization near proton stopping requires a reasonable approximation to the physical materials and thicknesses for the radiation transport code. The manufacturer provided a description of the metallization and passivation layers. Additional analyses were conducted to verify the back-end-of-line thickness, specifically the passivation layer, and that no additional material existed on top of those described. The analysis also determined the approximate fill factor of the heavier metal layers [48].

To support definition of model inputs, a focused ion beam was used to ablate sections of a die for inspection. The material cross section of the die was imaged by electron microscopy, as shown in Fig. 9. Six layers of metal above a silicon substrate are clearly visible in the center of the cross section. A thin passivation layer exists above the metallization, but no other layers are present. Optical microscopy was used to study the top metal layers in Fig. 10. The apparent metal fill pattern consumes a significant percentage of the upper BEOL.

Modeling of the material system can be done to varying degrees of accuracy in MRED. High-fidelity modeling can be done with a complete three-dimensional representation of the material system, including the fill patterns and metal traces for each layer of copper and vias descending through dielectric layers [3]. This type of model requires many Geant4 volumes, which in turn increases the burden of particle tracking just to capture the energy loss of the particle before it reaches the active silicon layers. A lower-fidelity model of the materials can be created with a multilayer, planar structure. This type of model contains layers of appropriate materials that vary in the Z direction, but are uniform in X and Y. While still three-dimensional,



Fig. 10. SRAM back end of line and metal fill under 100X magnification.

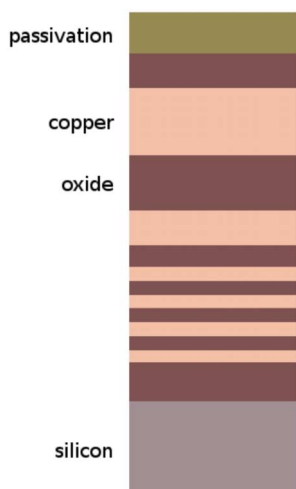


Fig. 11. Solid model representation of back end of line.

the details of the BEOL in the lateral dimensions are omitted. Each material layer is represented by a single rectangular parallelepiped (RPP), simplifying the Geant4 particle tracking. The metal layers have 100% fill factor in this representation, which has little effect on the energy deposition from electronic stopping.

Fig. 11 illustrates a two-dimensional view of the material stack used in this study. The silicon substrate thickness has been reduced for illustration. The inaccuracy in energy loss introduced by this assumption was determined to be small compared to other uncertainties within the full test setup, such as distance traveled and scattering encountered prior to reaching the die surface. The simplified planar structure may not be suitable for studies in which densities and types of materials in the BEOL greatly affect the probability of SEE through particle reactions, but it is useful to provide bounding scenarios.

2) *Calorimetry Using MRED*: Warren, *et al.* [49] developed a sensitive volume model in MRED using measured heavy ion SEU cross sections and then applied that model to predict proton and neutron responses. A similar approach was taken to model the 65 nm SRAM cell [41]. An SEU sensitive volume model is fundamentally a region or collection of regions that interpret

modeled energy deposition as collected charge. In this model, the criterion for producing an upset is defined such that simulated collected charge must be greater than the critical charge for upset. TCAD simulations and circuit simulations estimate the critical charge for upset for this SRAM to be 1.4 fC.

A weighted sensitive volume [50] was used to model SEU response in MRED.⁵ This model uses a complex set of volumes with defined charge collection efficiencies to mimic the increase in SEU cross section with LET. An initial set of volumes was constructed using heavy ion SEU data obtained at LBNL. The areal dimensions of the nested sensitive volumes were determined from measured heavy ion SEU cross sections. It was also assumed that the sensitive area was confined to the off-state NMOS transistor, and experimental effects of the off-state PMOS transistor from higher-LET particles would be lumped into this single region. The thickness of the sensitive volume was determined by the well geometry. Iterating over the dimensions of the sensitive volume and collection efficiencies refines the prediction of the heavy ion results.

3) *Proton-Induced SEU Simulation Results*: Fig. 8 compares the predicted proton-induced cross sections (red inverted triangles) with the measured data. The simulated SEU cross sections compare well to experimental data collected across the three facilities. While some discrepancies exist between 2 and 10 MeV, the mechanism for upset at energies below 2 MeV clearly shifts to direct ionization as evidenced by the large increase in the SEU cross sections.

In MRED simulations particle tracks may be selected based on physical interaction processes. Using this approach on the 65 nm SRAM showed that ionization from single protons caused upsets for low proton energies below 2 MeV, spallation events caused upsets for high-energy protons above 10 MeV, and a mix of interaction processes, including Coulomb scattering of single target elements, caused upsets between 2 and 10 MeV [41]. This level of insight into upset mechanisms is enabled by the detailed physical descriptions available in the simulation tools.

V. MODELING OF MUON-INDUCED SEUS IN SRAMS

The demonstration of the importance of direct proton ionization for the 65 nm SRAM in [41] and the availability of a corresponding, well-calibrated device model enabled the further investigation of the potential sensitivity of this and similarly sensitive devices to interactions with other lightly ionizing terrestrial particles. This is important to understand whether particles other than neutrons, which lead to indirect ionization in semiconductor devices, may also lead to significant contributions to error rates in terrestrial environments [51]. Protons are a component of the terrestrial cosmic ray environment. However, the abundance of low-energy protons in cosmic ray showers is relatively low. Other charged particles are present in larger quantities, and are now capable of being investigated with the calibrated MRED SEU model for the 65 nm SRAM of [41] by simply changing the particle species and kinetic energy within the simulation.

⁵The term “RADSAFE” in the title of [50] is essentially synonymous with “MRED,” and is no longer used.

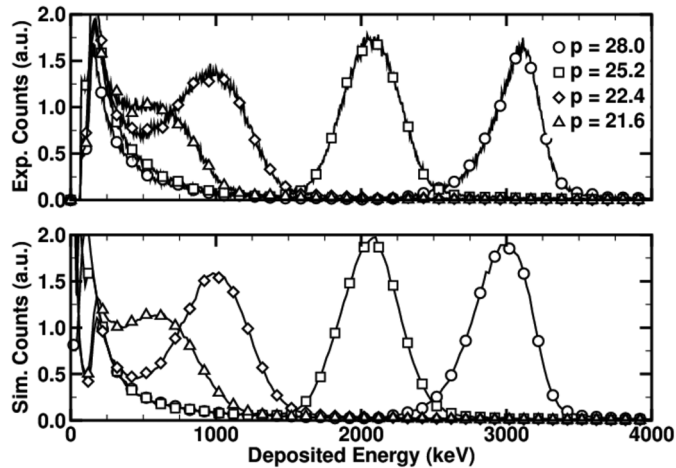


Fig. 12. Experimental (top) and MRED (V9 G4.9.4) simulated (bottom) energy deposition counts in 500 μm surface barrier detector. (After [52]).

Especially intriguing results were obtained when muons were investigated. The initial simulations suggested that a stopping muon could deposit enough charge in a bit cell to induce an upset similar to the stopping protons [52]. This prediction was a strong motivation to attempt a measurement. This is one of the first examples of basing an experimental test campaign entirely on a MRED prediction, as opposed to anomalies observed in ground testing. Test planning included simulations of the muon energies available at the proposed test facility, TRIUMF. Simple transport calculations were performed with MRED and the energy required for a muon to stop in the active silicon volume was estimated.

1) *Characterizing Muon Beams:* Monte Carlo simulations proved to be a valuable tool to aid in the characterization of the muon beam [52]. A surface barrier detector was placed in the beam prior to single event upset testing to observe the structure of the beam. Characterization of the muon beam by the facility had been performed at 28 MeV/c. Most muon science experiments carried out on the TRIUMF beam line have little reason to tune the beam in the manner that is done for microelectronics testing. Furthermore, the test required the use of a scintillator for dosimetry. The mean beam energy and spread at lower momenta after passing through the scintillator were measured.

A surface barrier detector (SBD) provided energy deposition events at each energy tune. The range of the muons in silicon was larger than the detector thickness. The energy of each event detected by the SBD was the combination of muons traversing the 500 μm detector and positrons introduced through muon decay. Pions were not detected, but if they had been present in the beam, they too would contribute to the energy deposition.

Simulation of the assumed initial beam momentum, energy spread through the scintillator, and the energy deposited in the SBD yielded energy deposition curves that were in good agreement with the experimental data, as shown in Fig. 12. Similar simulations of the beam line without the SBD informed the interpretation of the tests on the SRAM. The combination of experiment and simulation provided the calibration needed to characterize the SRAM muon-induced SEU cross section with respect to incident kinetic energy.

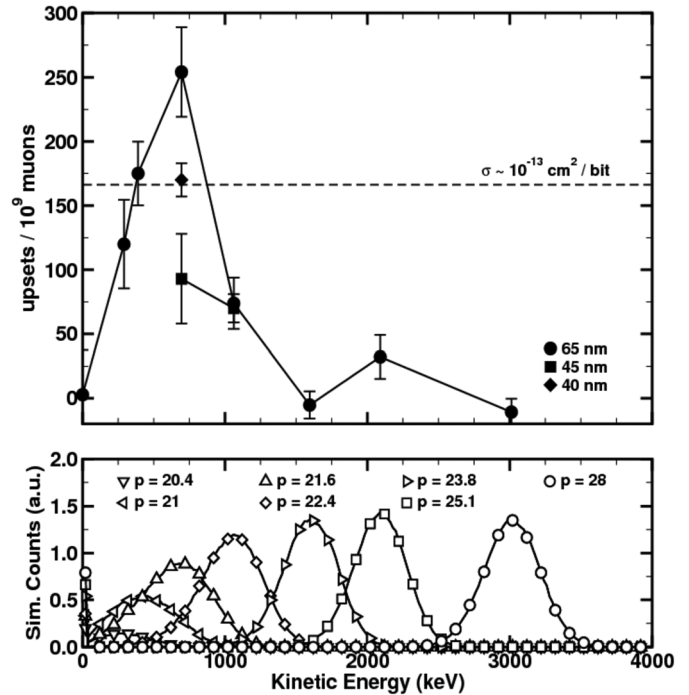


Fig. 13. MRED (V9 G4.9.4) simulations of the muon kinetic energy distributions, as seen at the front of the part, corresponding to experimental momentum including upstream energy losses and straggling (bottom). Error counts for 65 nm, 45 nm, and 40 nm SRAMs versus estimated muon kinetic energy at 1.0 V bias (top). Dashed horizontal line represents an approximate muon-induced SEU cross section. (After [52]).

2) *Experimental Confirmation of Muon-Induced SEUs:* Muon-induced single event upset cross sections have been experimentally measured at TRIUMF [53] and ISIS [54] with different manufacturers and technology nodes as summarized in [48], [52]. Fig. 13 presents the experimental upset probabilities versus muon kinetic energy measured at TRIUMF. The abscissa is related to the kinetic energy through the simulated beam energy distributions for each momentum tune. From these data, it is apparent that the majority of muon-induced upsets occur when a large portion of the muons traversing the active silicon are close to their Bragg peak and the collected charge is sufficient to exceed the SRAM critical charge. Above 1.5 MeV, the upset counts are indistinguishable from the background errors. Predictive simulations of the terrestrial muon-induced soft error rate for smaller technology nodes have demonstrated a strong dependence on the charge collection depth and critical charge. Rates range from insignificant for thin SOI volumes to greater than neutron error rates for deep bulk silicon collection [48], [52].

VI. MODELING OF ELECTRON-INDUCED SEUS IN SRAMS

Traditionally, the primary radiation effects caused by energetic electrons in the trapped radiation environments of Earth and Jupiter were considered to be total ionizing dose, displacement damage, and spacecraft charging [55], [56]. The decreasing critical charge of modern SRAMs has led to the emergence of SEUs induced by low-energy protons and muons, as discussed above. In recent years, interest has emerged in potential SEU effects due to high-energy secondary electrons

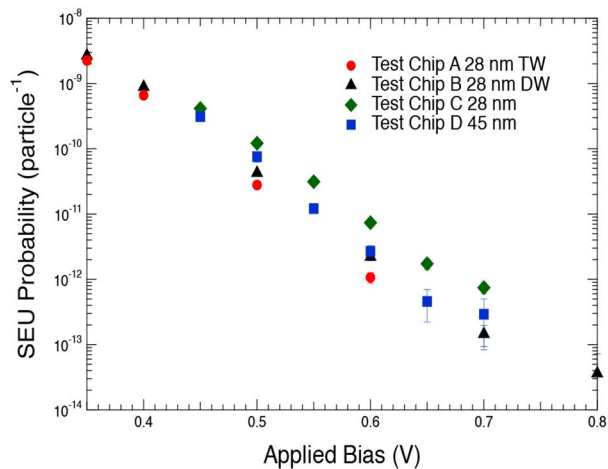


Fig. 14. Experimental errors induced during irradiation with 10-keV X-rays in an ARACOR Model 4100 X-ray irradiator. The bias sensitivity of critical charge in SRAMs provides strong evidence of energetic electron-induced upsets in modern SRAMs. (After [61]).

[57]–[60]. These secondary electrons, also called δ -rays, lose their kinetic energy through ionization, producing e-h pairs that may cause SEUs.

In [60] King *et al.* used MRED to predict that a single ionizing event from an energetic electron could deposit sufficient energy in a sensitive region of an advanced SRAM to cause an SEU. As a follow-on study, in [61] a low-energy X-ray source was used to generate energetic electrons to evaluate the susceptibility of CMOS SRAMs fabricated in 28 and 45 nm technology nodes to electron-induced SEUs. In this context, electron-induced SEUs refer to events where the initiating particle is a δ -ray. The resulting upsets are produced by thermalized e-h pairs generated as the δ -rays lose energy through ionization.

Upsets were observed within 10% of the nominal supply voltage conditions of a 28 nm technology. The assumption that these memory upsets are electron-induced SEUs was supported by further MRED simulations, which show that single energetic electrons deposit sufficient ionizing energy to generate charge in the sensitive volume of the device that is well in excess of estimated critical charge values. In [61] the impact of electron-induced SEU on error rates in space was explored as a function of technology feature size and voltage, and for ultra-low power applications. In [62] it was later demonstrated that indirect-ionization effects from 20 MeV primary electrons also produce SEUs.

1) *Experimental Results:* Results of exposing SRAMs fabricated in 28 and 45 nm technology nodes to a source of energetic electrons generated by X-ray-electron interactions, reported in [61], established that SRAMs may be sensitive to electron-induced SEUs under reduced supply voltage conditions. Fig. 14 plots the SEU probability per incident photon (computed by dividing σ by the number of bits in each memory, where σ is given by Equation 3 of [61]) as a function of supply voltage for SRAM test chips exposed to X-rays. Fig. 14 shows that errors are observed when these devices are biased between 0.35 V and 0.8 V while exposed to X-rays. The resulting upset probability of all test chips exhibits an exponential dependence on applied bias because of the dependence of critical charge on applied voltage.

This result is consistent with well-established test procedures used for assessing the SEU cross section for protons and muons [39], [52] and previous SEU results for alpha particles and heavier ions [63]–[65]. In the case of Test Chip B, upsets were observed within 10% of the nominal supply voltage of 0.9 V, which is within the designed operating voltage range for the SRAMs. Each of the SRAM test chips exhibits an SEU probability less than the total memory area on the die; this occurred at all supply voltages.

All observed errors had unique memory addresses, indicating that errors occurred randomly within the memory array during experiments and were not caused by repeated bit-flips in “weak” cells. No bit-flips occurred due to reduced bias conditions during functionality and parametric tests before and after X-ray irradiation of all test chips under all bias conditions, indicating the memory operated under stable conditions during experiments.

2) *MRED Simulations:* Radiation transport simulations were performed with MRED using the extensions that include PENELOPE 2008 (as described in the Section II) to evaluate the potential impact of electrons produced by energetic X-rays on the device SEU response. PENELOPE 2008 produces low energy electron trajectories that are more physical than available Geant4 classes, and therefore are assumed to provide greater spatial resolution. This increases the fidelity of energy deposition estimates in the small sensitive volumes relevant to 28 and 45 nm SRAMs. The incident X-ray spectrum described in [61], [66] was used to simulate the X-ray exposure environment and range of generated electron energies incident on the exposed SRAM test chip. A 4 Mbit SRAM array was simulated, using a sensitive volume structure consistent with a 45 nm bulk SRAM. Energy deposition was calculated for individual X-rays on an event-by-event basis. The sensitive volume geometry used was $0.22 \mu\text{m}^2 \times 500 \text{ nm}$, which is representative of 45 nm processes in the ITRS roadmap.

The simulated structure includes a 1 mm aluminum attenuator and appropriate BEOL thickness with $15 \mu\text{m}$ of oxide and metallization. The SRAM was simulated to a total photon fluence of $2 \times 10^9 \text{ cm}^{-2}$. This fluence was found to be sufficient to determine the energy deposited and estimate the resulting error rate with adequate precision to compare with the experimental data. The vertical black lines in Fig. 15 represent estimates of critical charge for 45 nm SRAMs as in [59] for supply voltages of 0.55 V and 1.1 V, which correspond to 0.19 fC and 0.38 fC, respectively, and are used to indicate the charge generation required to upset cells.

The simulated SEU probability of a 45 nm SRAM is shown in Fig. 15, indicating that secondary electrons generated by incident X-rays are capable of depositing sufficient energy to exceed critical charge estimations. The eventual upsets result from collection of thermalized e-h pairs generated by the high-energy electrons. These results, suggesting energetic electrons are capable of depositing sufficient ionizing energy to exceed the critical charge of 45 nm SRAMs operating under reduced supply voltage, are consistent with previous computational results reported in [59], [60]. The probability distribution shown in Fig. 15 at a supply voltage of 0.55 V agrees with experimental test results from Test Chip D in Fig. 14 within a factor of two. These results suggest that the 45 nm SRAM is sensitive to single elec-

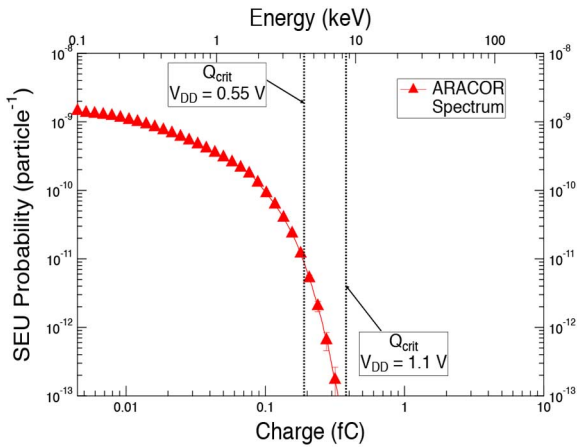


Fig. 15. MRED (V9 G4.9.4) simulation results of the attenuated ARACOR spectrum normally incident on a 45 nm bulk SRAM structure. The vertical black lines represent the lower-limit estimates of critical charge for a 45 nm SRAM. The results provide supporting evidence suggesting that energetic electrons generated by incident X-rays are capable of depositing sufficient energy to exceed the estimated upset threshold. (After [61]).

tron-induced SEU at reduced supply voltage, consistent with the SEU data in Fig. 14. These simulation results confirm that energy deposition from energetic electrons generated in photo-absorption events is the most likely explanation for the experimentally observed upsets in Fig. 14.

3) *Electron-Induced On-Orbit Error Rates*: To quantify the relative significance of electron-induced SEUs relative to populations of other particle species, one must look at the associated error rates of these particles for different environments and compare the total error rate to that of energetic electrons. Trapped electrons form two different belts in the near-Earth radiation environment, each with distinct characteristics [55], [56]. The Jovian electron environment is even more formidable as it contains electrons with higher energy and flux than that of the near-Earth environment. Next, we explore the potential for electron-induced SEUs in the near-Earth and Jovian environments.

MRED simulations were performed to estimate SEU event rates for trapped electrons at geosynchronous orbit during solar maximum with 150 mils of aluminum shielding using spectra obtained from the AE-8 model for the near-Earth environment. The differential flux spectrum of incident electrons through 150 mils of Al shielding is shown in Fig. 16. The trapped electron environment described in [61], [67] is much more energetic than the generated electron spectrum used in X-ray experiments described above and analyzed more thoroughly in [61], [66]. The most energetic electrons at geosynchronous orbit during solar maximum have energy of approximately 10 MeV, which require more than 500 mils of Al shielding to attenuate completely [55], [56].

The material structure used for the MRED simulations is identical to that of the devices under test in Fig. 15, corresponding to a 45 nm bulk SRAM. Fig. 17 shows the resulting simulated event rates (left/right axis) as a function of generated charge (bottom axis) or energy deposited (top axis) within the sensitive volume of a single 45 nm SRAM cell for the near-Earth environment. The vertical lines shown in Fig. 17 are

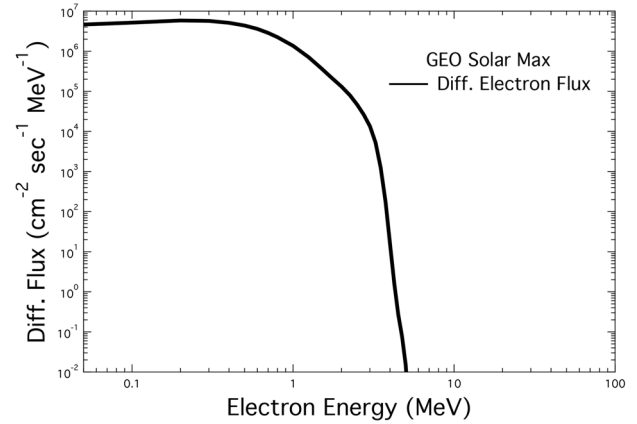


Fig. 16. MRED (V9 G4.9.4) simulations performed on the 45 nm structure from Fig. 14 using the AE-8 description of the electron environment, at geosynchronous orbit during solar maximum with 150 mils aluminum shielding. The differential flux spectrum of incident electrons is plotted. (After [61]).

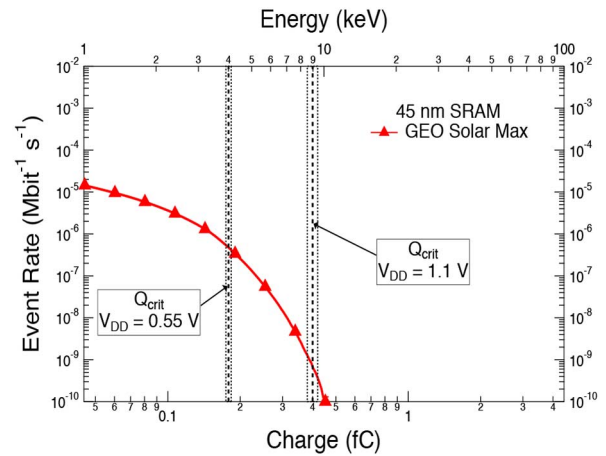


Fig. 17. MRED (V9 G4.9.4) simulations performed on a 45 nm SRAM structure using the AE-8 description of the electron environment, at geosynchronous orbit during solar maximum with 150 mils aluminum shielding. Simulation results show that the event rate of electrons is small for devices operated at nominal supply voltage. However, more sensitive devices will experience a significant increase in single electron events. These results suggest that operating SRAMs under reduced bias conditions will result in a dramatic increase in single electron events. (After [61]).

the critical charge of a 45 nm SRAM and indicate the expected error rates for 45 nm SRAMs operating at 0.55 V and 1.1 V at geosynchronous orbit. Electron energy deposition events rarely exceed 10 keV, which is consistent with Fig. 15 and previous studies of δ -rays [59], [60]. Fig. 17 demonstrates the rare nature of electron-induced SEU events in the near-Earth space radiation environment, indicating that many years of flight time may elapse before the observation of such an event is expected for a typical 45 nm bulk SRAM operating under nominal bias conditions.

Fig. 17 shows that electron-induced SEU event rates depend strongly on the critical charge of the SRAM; a reduction of critical charge from 0.4 fC to 0.2 fC results in a change in event rate of approximately two orders of magnitude. Employing more sensitive SRAM technologies or operating at reduced supply voltages has a direct and significant impact on SRAM error rates. In contrast, total error rate predictions for a 65 nm SRAM

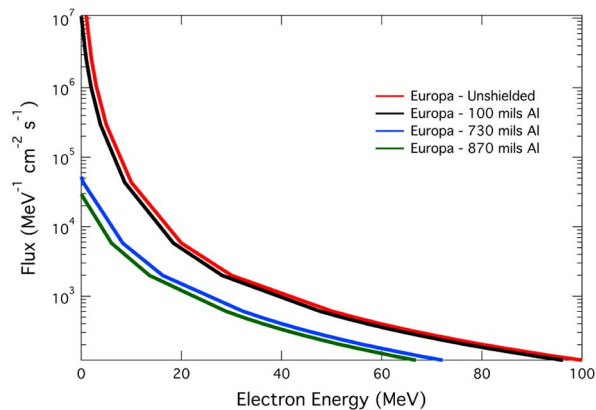


Fig. 18. Differential electron flux for unshielded, 100 mils, 730 mils, and 870 mils of aluminum shielding in the Europa tour phase of the Juno spacecraft mission to the Jupiter planetary system.

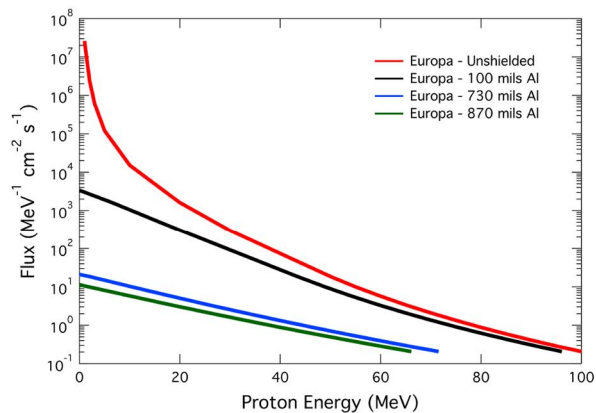


Fig. 19. Differential proton flux for unshielded, 100 mils, 730 mils, and 870 mils of aluminum shielding in the Europa tour phase of the Juno spacecraft mission to the Jupiter planetary system.

at geosynchronous orbit in the solar minimum environment are $\sim 2.4 \times 10^{-6} \text{ Mbit}^{-1}\text{s}^{-1}$, and in the “worst-day” environment the error rates for the same 65 nm SRAM are as high as $3.6 \times 10^{-3} \text{ Mbit}^{-1}\text{s}^{-1}$ [41]. This indicates that error rates at geosynchronous orbit for larger technology nodes with higher critical charge are roughly 2.5 to 5 orders of magnitude higher than estimates of electron-induced error rates at nominal bias conditions.

Characteristics of the Jovian electron environment can be found in [67]. Simulations of electron-induced SEU event rates were performed for the differential flux spectrum of electrons and protons during the Europa tour of the planned Juno NASA mission to the Jupiter planetary system. The electron flux spectrum during the Europa tour is shown in Fig. 18, and indicates that 100 mils of Al shielding has minimal impact on the flux of low-energy electrons ($< 100 \text{ keV}$). The proposed higher shielding thicknesses of 730 and 870 mils, however, have a larger impact on the flux of low-energy electrons, reducing it by over two orders of magnitude, as seen in Fig. 18. In contrast to electrons, shielding of protons has a much greater impact on the proton flux in the Europa environment (Fig. 19), reducing the high-flux region of low-energy ($< 5 \text{ MeV}$) protons from the unshielded spectrum.

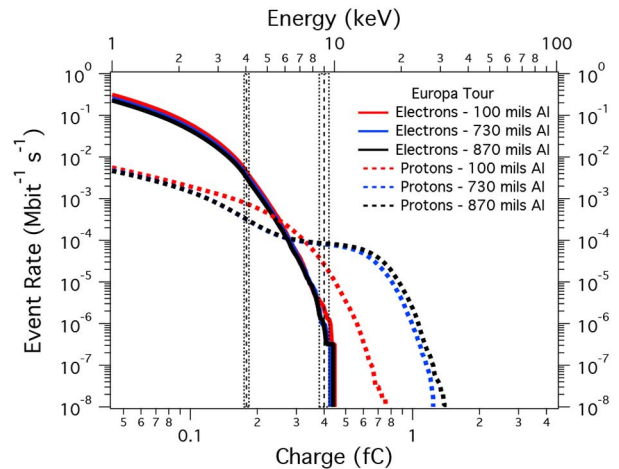


Fig. 20. MRED (V9 G4.9.4) simulations performed on the 45 nm SRAM structure using the Europa tour electron and proton environment for shielding thicknesses of 100, 730, and 870 mils of aluminum. Proton-induced SEU error rates are observed to be higher than electron-induced SEU error rates at nominal supply voltage. Electron-induced SEU error rates become higher than proton-induced error rates under reduced bias conditions.

Rate prediction conclusions are similar for the Jovian trapped particle environment to those of the near-Earth environment when evaluating SEU error rate estimations. The vertical lines shown in Fig. 20 are again the critical charge of a 45 nm SRAM discussed previously and indicate the expected error rates for 45 nm SRAMs operating at 0.55 V and 1.1 V in the Jovian environment. The solid lines in Fig. 20 show the electron-induced SEU error rate calculated by MRED simulations using the differential electron flux in the Europa environment for shielding thicknesses of 100, 730, and 870 mils of aluminum. Results show that shielding has some impact on the overall electron-induced SEU error rate in the Europa environment, as shown by the slight reduction in event rates. The difference in error rates for increasing shielding thicknesses appears to be negligible near nominal operating voltages for the 45 nm SRAM test chip, while there is some indication that thicker shielding decreases the SEU error rate slightly under reduced bias conditions. Increasing shield thickness appears to provide diminishing returns for attenuating the electron-induced SEU error rate near Jupiter and Europa, as it is impractical to use sufficient shielding to stop the 100 MeV electrons present in those environments. Devices operated in a low-power or quiescent mode are likely to experience an unacceptably large upset rates while in proximity to the Jupiter planetary system.

The dashed lines in Fig. 20 show MRED simulation results for a 45 nm SRAM exposed to the proton environment around Europa for shielding thicknesses of 100, 730, and 870 mils of aluminum. Proton-induced SEU error rates are higher than electron-induced SEU error rates at nominal supply voltage conditions. While the proton flux is significantly attenuated by the presence of the aluminum shielding, this results in a proton spectrum that is more likely to cause bit-flips within the SRAM cell. This is shown by the slight increase in event rate for shielding thicknesses of 730 and 870 mils, as compared to 100 mils. Interestingly, Fig. 20 suggests that electron-induced SEU error rates are estimated to be higher than proton-induced error rates under a range of reduced bias conditions.

Comparing electron-induced SEU error rates for near-Earth and Jovian environments yields consistent results. Although the environments are dramatically different, the calculated SEU error rates suggest that electron-induced SEUs at or near nominal bias conditions are extremely rare events and unlikely to contribute to error rates in SRAMs fabricated in technology nodes at or above 45 nm. The presence of high fluxes of energetic electrons, up to 100 MeV, has a significant impact on error rates, especially under reduced bias conditions, in the Jovian environment when compared to that of lower energy electrons found in the Van Allen radiation belts.

The differences between the Jovian and near-Earth environments are most significant at reduced bias conditions where electron-induced SEU error rates are higher than those of the geosynchronous environment by more than an order of magnitude. Furthermore, the estimated error rates in Fig. 17 and Fig. 20 suggest that spacecraft operating near an energetic electron environment, like those found in the Van Allen radiation belts or the Jupiter planetary system, that enter into a power-saving or quiescent mode would significantly increase the likelihood of SEUs contributing to anomalous behavior in the onboard electronics systems.

VII. MODELING OF MULTIPLE-CELL UPSETS

Multiple-cell upsets (MCUs) are events in which a single particle changes the state of more than one memory element. If the affected cells are in the same logical word, the event is described as a multiple-bit upset (MBU). Monte Carlo simulation is well suited for predicting and analyzing MCU because of its ability to track all of the secondary, tertiary, and subsequent-generation particles resulting from the interaction of a single primary particle [68]. Each one of these particles has the potential to affect one or more cells, possibly resulting in large clusters of errors from a single primary particle.

If one particle upsets several cells, but each affected cell is in a different word, all of the errors can be corrected by simple error detection and correction (EDAC) schemes [69]. If the affected cells are in the same word, however, the errors may not be correctable without use of more sophisticated techniques. Consequently, MBUs are particularly important in determining the reliability of advanced memories. Spatially separating bits in a word can help to reduce the likelihood of MBUs. Monte Carlo analysis can be used to determine how effective this separation will be for a given technology and radiation environment.

Scaling of integrated circuits has decreased the amount of charge required to upset storage cells. The sensitive volume per bit has also decreased, which tends to reduce the SEE cross section. These competing effects have led to complicated SEE responses in highly-scaled technologies. For proton irradiation of bulk CMOS technologies, little or no change in SEU rates is typically observed, while multiple-bit upset rates increase [70]. Additionally, proton ground testing does not account for device orientation or angle of incidence [71]. The probability of MCU in various technologies has been reported, showing that the fraction of single events that leads to MCU increases for smaller technologies [72]–[77].

In [68], a TCAD model of an SRAM was imported into MRED. This is a useful demonstration of how Monte Carlo

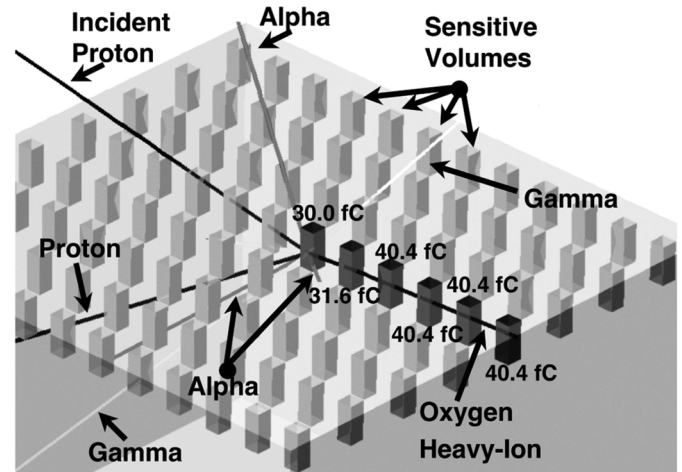


Fig. 21. A MRED-(V7 G4.8.0) generated nuclear event initiated by a 63-MeV proton in silicon. Each shaded volume represents the sensitive volume of a single cell. 30 fC or more charge is generated in each of six cell volumes. After [68].

simulations can be used to analyze multiple-cell or multiple-bit upsets. An array of 204 sensitive volumes, equivalent to the sensitive volumes in a $20 \mu\text{m} \times 20 \mu\text{m}$ area, was used to represent the SRAM cells. The SRAM cell dimensions were $1.9 \mu\text{m} \times 1.3 \mu\text{m}$. Upsets produced by 63 MeV and 200 MeV protons were analyzed. For each proton event, MRED recorded the energy deposited in each sensitive volume by the primary proton and secondary particles. For example, Fig. 21 shows a single nuclear reaction initiated by a 63 MeV proton. MRED computes the energy deposited in multiple sensitive volumes by the energetic residual oxygen ion resulting from the nuclear reaction. The energy deposition cross section is defined as

$$\sigma_{ED}(E) = \frac{N}{\phi}$$

where N is the number of events that deposit energy E or greater in the sensitive volume and ϕ is the fluence. The SEU cross section is the value of σ_{ED} that corresponds to the critical charge. The multiple volume energy deposition cross section is defined as

$$\sigma_{MBU} = \sigma_M(Q_{crit})$$

where σ_M is the cross section to deposit a given amount of charge in two or more sensitive volumes.

The simulation results for multiple cell events are shown in Fig. 22 and Fig. 23 for 63 and 200 MeV protons, respectively. The angular dependence for the lower energy protons is much greater than that for the higher energy protons. For the 63 MeV protons, the MBU cross section increases with angle due to the longitudinal scattering of secondary products in the sensitive volume plane. For this energy, protons normally incident to the sensitive volume plane produce secondary particles that travel into the silicon bulk and away from the sensitive region, traversing a minimal number of sensitive volumes. As the angle of incidence increases, the scattered products travel in the plane

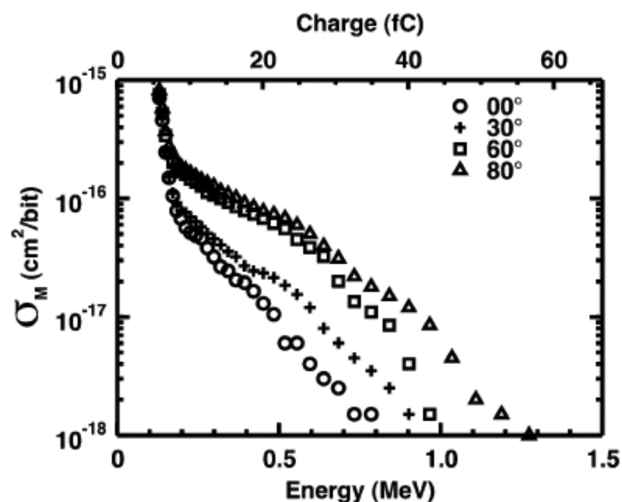


Fig. 22. MRED (V7 G4.8.0) simulation of multiple volume energy deposition cross sections for 63 MeV protons. (After [68]).

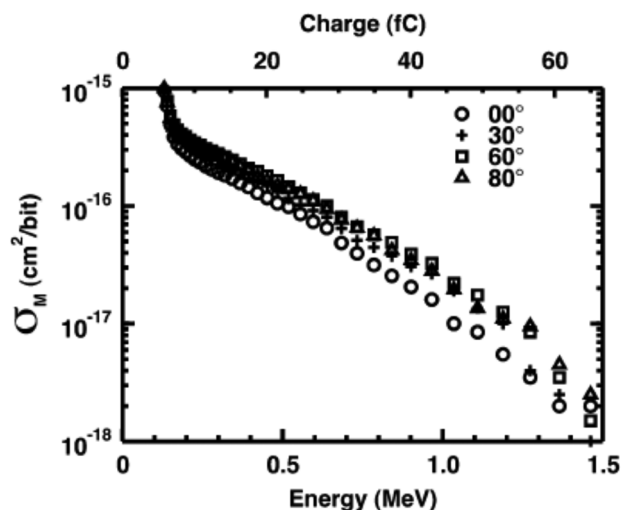


Fig. 23. MRED (V7 G4.8.0) simulation of multiple volume energy deposition cross sections for 200 MeV protons. (After [68]).

containing the sensitive volumes and the MBU probability increases. For the 200 MeV particles, the distribution of secondary products is much less sensitive to angle. Experiments along with MRED simulations for protons [78] and neutrons [79] have been used to estimate the probability of observing MCUs for space and terrestrial radiation environments.

VIII. MODELING TID ENHANCEMENT DUE TO HIGH-Z MATERIALS NEAR OXIDES

MRED also has been applied to evaluate effects of the total ionizing dose (TID) deposited in gate insulators encapsulated with layers of materials of varying atomic number, which are typical of past, present, and future generations of micro-electronic devices and ICs. The effects of 10-keV X-rays and 400-keV endpoint-energy bremsstrahlung X-rays on MOS capacitors with SiO_2 or HfO_2 gate dielectrics and Al and TaSi gate metallization have been studied in particular detail. As validation, calculations have been compared with previous results in the literature obtained with other Monte Carlo and

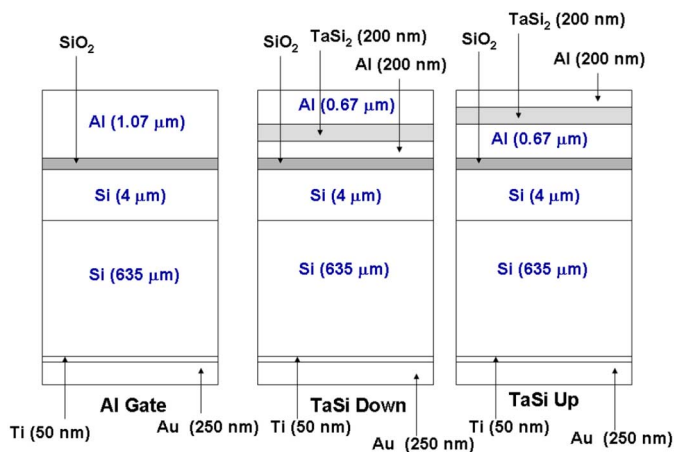


Fig. 24. Device geometries for Al-gate, TaSi₂-down, and TaSi₂-up MOS capacitors. (After [81]).

discrete ordinates codes, and with experiments on devices with SiO_2 gate dielectrics, with generally good agreement [80].

Schematic diagrams of MOS capacitors having three different geometries are shown in Fig. 24. These include capacitors with a SiO_2 gate dielectric and a pure Al gate, and structures with two different configurations of Al and TaSi that were fabricated at Sandia National Laboratories [81], [82]. The thicker oxides are useful for comparing predicted and experimental values for the equilibrium doses in dielectrics. The ultra-thin gate dielectrics are more relevant for comparison to results for present and future generations of MOS technologies.

Each structure in Fig. 24 was simulated using MRED. The implementation of low energy electromagnetic processes in this particular Geant4 toolkit [4], [5] is valid for energies down to 250 eV and can be used up to approximately 100 GeV. The output of this version of MRED was compared with the Geant4 low energy electromagnetic physics models for electron transport with a version that incorporates the electron transport code PENELOPE 2008 [19]–[24]. Calculations with these two methods differed by less than the experimental variations in device response that were noted in [81], [82]. In the comparisons between calculations and experiment that follow, we present the averages of the two calculated values.

Fig. 25 shows the dose enhancement factor (DEF) calculated for the structures of Fig. 24 for irradiation with 10-keV X-rays, relative to the equilibrium dose that would otherwise have been deposited in a slab of pure SiO_2 of equivalent thickness. The doses for thin oxides are greater than those in thicker oxides because of the secondary electrons generated within surrounding higher-Z layers that have a relatively limited range in SiO_2 [81], [83], [84]. Hence, the DEF values increase monotonically with decreasing gate oxide thickness for all three geometries and converge for the thickest (~ 1060 nm) oxide, consistent with expectations based on previous experimental and theoretical studies of interface dose enhancement in MOS devices and materials [81], [83], [84]. MRED calculations of dose enhancement have been compared with predictions of earlier-generation Monte Carlo and discrete ordinates codes that were in use in the 1980s [81], and found to be generally consistent or superior to these earlier estimates as a result of enhanced computational

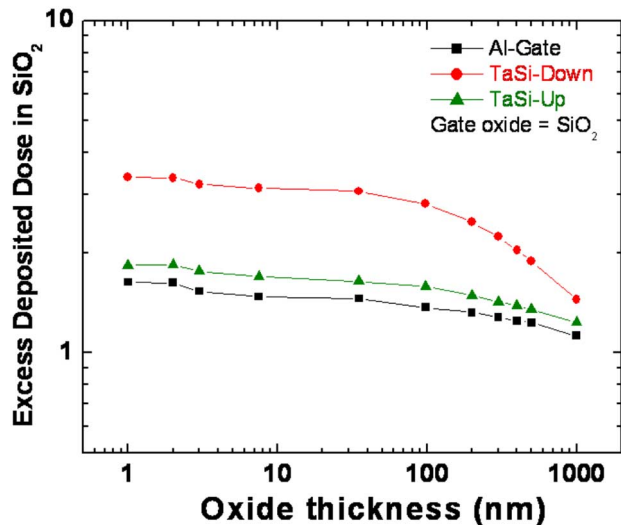


Fig. 25. MRED (V9 G4.9.4) simulation of enhanced dose due to 10-keV X-rays for the MOS capacitor structures of Fig. 19 as a function of SiO₂ dielectric layer thickness. The excess dose (dose enhancement) is defined here as the ratio between the SiO₂ dose in the gate oxide layer to the dose deposited in the same sensitive SiO₂ volume in a block of pure SiO₂. (After [80]).

capabilities and updated physical models that are now available [80].

To facilitate comparisons between code calculations and experimental values that are independent of dosimetry, charge yield, differences in trapping efficiency, and other factors that complicate the general prediction of TID response [80], [85], Fig. 26 compares MRED calculations of the ratio between the calculated DEFs presented in Fig. 20 for 10-keV X-rays for capacitors with 35 nm oxides to those for 1060 nm oxides. These are compared with the experimentally measured ratios of hole trapping reported in [81] for capacitors with oxides of these two thicknesses. Fig. 26 shows that MRED calculations of the enhanced dose due to the higher-Z overlayers match well the experimentally measured values, supporting the ability of the code to calculate both the effects of the incident particles and the subsequently generated secondary particles on the resulting TID in the sensitive volume of interest [80].

Fig. 27 shows the ratio of the calculated dose in capacitors with the SiO₂ gate dielectric layer of the capacitor structures of Fig. 19 replaced with HfO₂ to the equilibrium dose in a thick SiO₂ gate dielectric, again for 10-keV X-rays. Now, instead of an enhanced dose, we see dose reduction in the HfO₂ for thinner dielectric layers. This occurs because much of the energy initially deposited in this higher-Z HfO₂ layer now transports via the generation of secondary electrons to the surrounding lower-Z gate and substrate materials. For HfO₂ layer thicknesses of technological interest (2 to 4 nm), these calculations show that the dose in the gate dielectric after electron transport is $\sim 2 - 3$ times higher than the equilibrium dose in SiO₂ [80], [86]. The accuracy of these calculations are compared with analytical calculations in [80] and experimental measurements in [87], with good agreement found. MRED estimates of the complex interactions among high-K dielectric layers and back-end-of-line (BEOL) materials are presented in [86], with dose enhancement observed in some cases, and

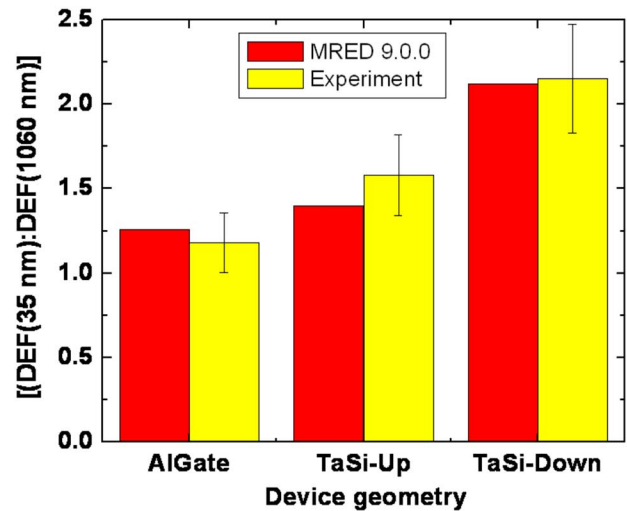


Fig. 26. MRED (V9 G4.9.4) calculations of the ratios of the DEFs due to 10-keV X-rays for capacitors with 35 nm oxides to the DEFs of capacitors with 1060 nm oxides. These are compared with the experimentally measured ratios of hole trapping reported in [81] for capacitors with oxides of these two thicknesses. (After [80], [81]).

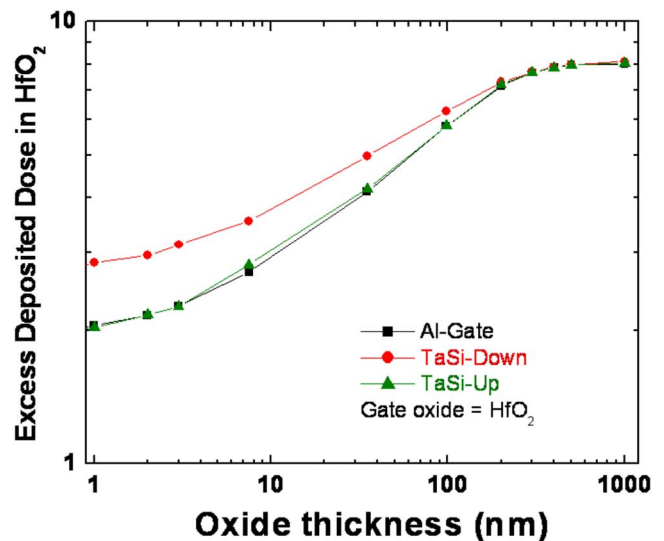


Fig. 27. MRED (V9 G4.9.4) simulation of excess dose deposited in HfO₂ MOS capacitor structures compared to the equilibrium deposited dose in a pure SiO₂ structure due to 10-keV X-rays. The dose reduction in the gate dielectric observed for thin HfO₂ layers is significantly greater when the dielectric is surrounded by lower-Z materials than when surrounded by higher-Z materials. (After [80]).

dose reduction observed in others, depending on the respective dielectric and BEOL materials and layer thicknesses.

Fig. 28 shows MRED calculations of dose enhancement for the capacitors of Fig. 24 with SiO₂ gate dielectrics or HfO₂ gate dielectrics irradiated with a 400-keV endpoint bremsstrahlung spectrum that is described in [80], [82]. Much higher doses are deposited in the HfO₂ MOS capacitors as compared to the SiO₂ MOS capacitors for the entire range of oxide thicknesses. The dose deposited in the thickest HfO₂ capacitor is ~ 10 times that for the thickest SiO₂ layer capacitor. To compare with previous work, where possible, we note that the doses in the TaSi₂-down capacitors with SiO₂ dielectric layers in Fig. 28 are $\sim 1.9 - 2.3$

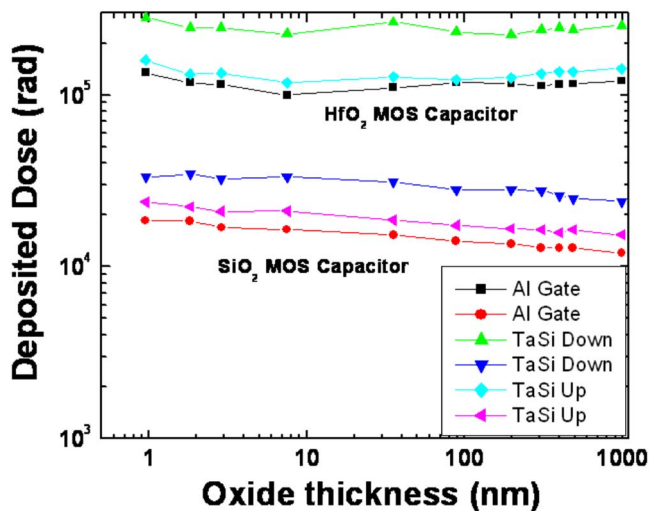


Fig. 28. MRED (V9 G4.9.4) simulation of dose (in rad(SiO_2) and rad(HfO_2)) as a function of physical oxide thickness for HfO_2 and SiO_2 gate dielectric layers for the MOS capacitor structures of Fig. 19, for a 400-keV endpoint-energy bremsstrahlung X-ray spectrum. (After [80]).

times higher than the doses in the Al-gate capacitors. The measured ratios for the comparable experimental device responses in [82] are $\sim 1.9 - 2.1$. These experiments were done on similar Al-gate and TaSi₂-gate capacitors at 300 K, using the Sandia Pelletron to generate a 400-keV endpoint-energy bremsstrahlung X-ray spectrum [82]. The MRED calculations for SiO_2 also match well the DEFs of $\sim 2.0 - 2.3$ predicted by the integrated-Tiger-series coupled electron/photon transport codes in [82]. These results demonstrate that MRED calculations of TID effects in dielectric layers can be quite helpful to understanding dose enhancement phenomena [80], [85]. Consequently, they also strongly demonstrate that MRED is calculating the total energy deposition in sensitive volumes of microelectronic materials and devices with accuracy comparable to that possible in experimental studies.

IX. MODELING OF DISPLACEMENT DAMAGE

Displacement damage occurs when an incident particle displaces atoms as it travels through a semiconductor lattice. The resulting stable, electrically active defects are detrimental to device performance metrics such as BJT gain, light emission in LEDs, diode leakage current, and CCD pixel dark current. A thorough review of displacement damage physics, modeling, and device effects can be found in [88]. MRED has been used to model the average amount of displacement damage sustained by proton-irradiated GaAs [89] and heavy ion-irradiated Si [90]. MRED has also been used to calculate the distribution of displacement damage in proton-irradiated HgCdTe [91] and heavy-ion-irradiated Si [92].

A. MRED Simulations of Average Displacement Damage

Radiation-induced degradation in many semiconductor devices has been shown to scale with nonionizing energy loss (NIEL). NIEL is a calculated metric that represents the average amount of nonionizing energy that an incident particle loses to

the creation of lattice damage. NIEL is calculated in units of $\text{MeV cm}^2/\text{mg}$ as

$$NIEL(E) = \frac{N}{A} \int \int_{\theta_{min}}^{\pi} \left(\frac{d\sigma(\theta, E)}{d\Omega} \right) T(\theta, E) L[T(\theta, E)] d\Omega \quad (1)$$

where E is the energy of the incident particle, N is Avogadro's number, A is atomic mass of the target material, θ is the recoil scattering angle, $d\sigma/d\Omega$ is the differential cross section for atomic displacements, T is the average recoil energy, and L is the Lindhard partition function [93]. Methods to calculate NIEL have been presented in [94]–[97].

NIEL calculations quantify nonionizing energy loss averaged along a particle trajectory. By contrast, MRED tallies the nonionizing energy deposited by a particle within a device in three spatial dimensions. This preserves position-dependent information about atomic displacement, atomic stopping, and phonon generation. Although an atomic collision may take place outside of a depletion region, the location of the resulting displacement damage may occur within a depletion region where it will have damaging effects on device performance.

MRED calculates the nonionizing energy deposited per unit volume by an incident particle as a field $F(\vec{z}, \vec{p}; \vec{x})$. Here \vec{z} is the initial position of the incident particle, \vec{p} is the momentum of the incident particle, and \vec{x} is the location where the nonionizing energy is deposited [89]. The nonionizing energy deposition rate, η , of the incident particle can be calculated by integrating the field $F(\vec{z}, \vec{p}; \vec{x})$ over x and y :

$$NIEL(E(p, z)) \simeq \eta(p, z) = \int \int F(\vec{0}, p\hat{k}, z\hat{k}) dx dy \quad (2)$$

B. Comparison of MRED Estimate of Nonionizing Energy Deposition Rate to Experimental Damage Factors

1) *Light Emission Reduction in GaAs LEDs:* In [89], the reduction in minority carrier lifetime observed in GaAs LEDs irradiated with 1 to 500 MeV protons and reported in [98] was compared to nonionizing energy deposition rates calculated with MRED as well as NIEL values calculated with the methods described by Burke [96] and Jun [97]. Energy-dependent nonionizing energy deposition rates from MRED were subdivided into contributions from relativistic Coulomb interactions and nuclear recoils (both elastic and inelastic). NIEL values were calculated from nonionizing energy lost through nuclear recoils. Fig. 29 compares NIEL values to GaAs LED damage for proton energies between 1 MeV and 1000 MeV.

The reductions in minority carrier lifetime observed in GaAs LEDs irradiated with 1 to 10 MeV protons agreed well with non-ionizing energy deposition rates computed with MRED [89]. In fact, the minority carrier lifetime damage factor scaled with nonionizing energy deposition rate calculations from relativistic Coulomb interactions for the tested proton energy range of 1 MeV to 500 MeV. However, the NIEL values overestimated GaAs damage by a factor of 10 for 500 MeV protons. Nonionizing energy deposition rates calculated from nuclear recoils overestimated GaAs damage by a factor of 2 for 500 MeV protons.

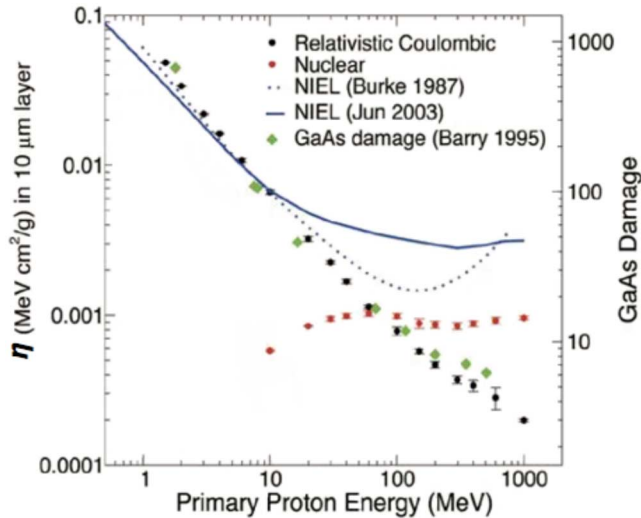


Fig. 29. Comparison of MRED (V6 G4.6.0) calculations of nonionizing energy deposition rate (η) to NIEL calculations and experimental results from proton testing on GaAs LEDs. (After [89]).

2) *Leakage Current Increase in Si JFET Diodes:* In [90] the total increase in leakage current was measured in Si JFET diodes irradiated with ^{252}Cf and ^{241}Am . The ^{241}Am source emits 5.9 MeV alpha particles, and ^{252}Cf emission byproducts include 5.6 MeV alpha particles, neutrons with an average energy of 0.5 MeV and peak energy of 2 MeV, and light and heavy fission fragments. A typical ^{252}Cf light fission fragment is 106 MeV Cd, and a typical heavy fragment is 80 MeV Nd. Damage factors for both diodes were defined as the average increase in leakage current per particle. The damage factors were calculated to be 1.2 fA per fission fragment for the ^{252}Cf -irradiated diode and 1.9×10^{-3} fA per alpha particle for the ^{241}Am -irradiated diode. Fig. 30 compares the ratio of experimental damage factors measured for fission fragments and alpha particles to the ratios of NIEL values calculated with SRIM and MRED for the same ion species and energies.

The ratio of NIEL values for two types of particle incident upon the same target material is equal to the ratio of damage measured after irradiation with those two types of particles [99]. The nonionizing energy deposition rate was calculated for 106 MeV Cd and 80 MeV Nd in Si using MRED as described in [89]. The average nonionizing energy deposition rates for these two fission fragments was divided by the nonionizing energy deposition rate calculated for 5.9 MeV alpha particles in Si. Similarly, NIEL values for 106 MeV Cd and 80 MeV Nd in Si were calculated with SRIM using the method described in [95]. The average of these two values was divided by the NIEL value for 5.9 MeV alpha particles in Si. The ratio of damage factors measured in the ^{252}Cf -irradiated diode and the ^{241}Am -irradiated diode was within 6% of the NIEL ratio calculated with SRIM and within 12% of the nonionizing energy deposition rate value calculated with MRED [90].

C. Displacement Damage Distributions

Although the average amount of nonionizing energy can be used to predict device degradation for a given fluence, neither NIEL nor the nonionizing energy deposition rate computed

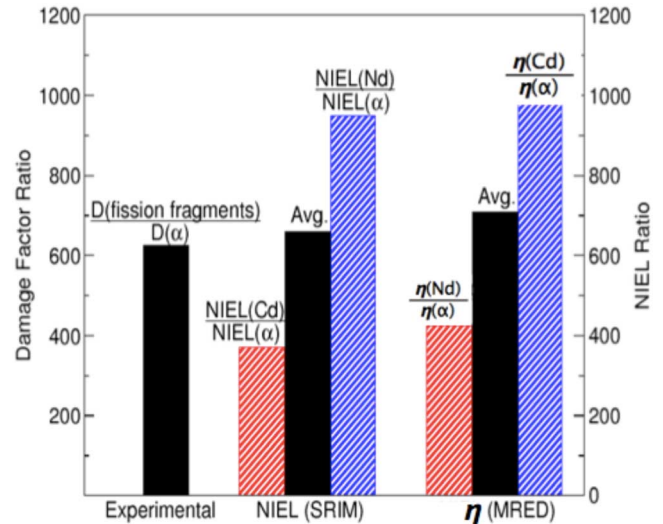


Fig. 30. Ratios of experimental damage factors and NIEL values calculated with SRIM and MRED (V9 G4.9.4) for Si JFET diodes irradiated with fission fragments emitted by a ^{252}Cf source and alpha particles emitted by an ^{241}Am source. (After [90]).

from MRED can always accurately predict how much the amount of displacement damage will vary between individual particles. Distributions of degradation events caused by individual energetic particles include “extreme” events that do not scale linearly with NIEL. The maximum sizes of damage events measured in different materials exceed the maximum values predicted by the kinematics of atomic collisions [98], [99]. MRED has been used to demonstrate that the distribution of damage calculated for proton-irradiated HgCdTe CCD pixels underestimates the measured distribution of dark current increases [91]. In addition, MRED calculations of location-dependent vacancies and interstitial atoms have also been used to predict the distribution of leakage current increases in heavy ion-irradiated Si JFET diodes when electric field enhancement is suspected to be present [92].

1) *Distribution of Dark Current Increase in HgCdTe Pixels:* In [91], dark current increases were measured in 266,000 HgCdTe pixels irradiated with 63 MeV protons to predict on-orbit radiation damage for the James Webb Space Telescope. Probability distributions for Coulomb interactions, nuclear elastic reactions, and nuclear inelastic reactions were compared to a probability distribution function describing dark current increase in the irradiated pixels. The relativistic Coulomb interaction contribution to nonionizing energy was calculated with MRED. Nuclear elastic and inelastic contributions to nonionizing energy deposition were calculated with the MCNPX code [100].

A comparison of probability distribution functions for the measured increases in pixel dark current and calculated quantities of nonionizing energy loss per pixel demonstrated that the maximum size of extreme damage events cannot be predicted from NIEL, as shown in Fig. 31. The largest measured increase in dark current (0.1 electrons/s) was twice the size of the largest predicted increase (0.05 electrons/s). In addition, nonionizing energy calculations underestimated the number of pixels predicted to sustain extreme damage. Only 3 pixels were predicted

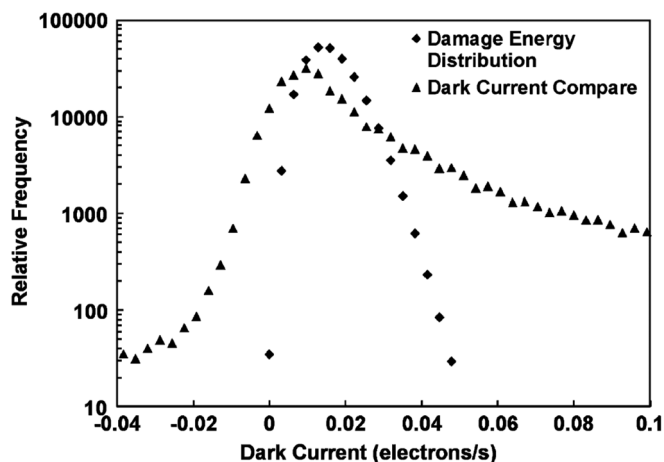


Fig. 31. Histogram comparing the dark current increases measured in proton-irradiated HgCdTe pixels with the damage energy distribution calculated with MRED (V8 G4.8.1) and MCNPX. (After [91]).

to sustain a dark current increase of 0.05 electrons/s, but dark current increases of this magnitude were measured in approximately 3,000 pixels. Electric field enhancement was stated as a possible mechanism for the extreme dark current increases observed in the HgCdTe pixels.

2) *Distribution of Leakage Current Increase in Si JFET Diodes:* Single ion-induced increases in leakage current were measured in three Si JFET diodes exposed to a ^{252}Cf source [92]. The distribution of measured leakage current increases was compared to the distributions of calculated leakage current increases expected from Frenkel pairs created by 106 MeV Nd and 80 MeV Cd ions, typical light and heavy fission fragments emitted by a ^{252}Cf source. MRED was used to identify the location of atomic displacement sites (vacancies) and stopped atoms (interstitials) within the depletion regions of a Si JFET diode. The increased defect density resulting from these vacancies and interstitials was used to calculate the decrease in generation lifetime caused by damage from individual ions. The expression for Shockley-Read-Hall generation was used to calculate a distribution of leakage current increases [101].

The increase in defect density alone was insufficient to account for the measured distribution of leakage current increases. However, electric field simulations performed with Silvaco TCAD identified volumes within the Si JFET diodes in which electric field strength exceeded 10^5 V/cm. When electric field enhancement was applied to the Shockley-Read-Hall generation rates of defects located in high electric field regions, the distribution of leakage current increases predicted from individual 106 MeV Nd and 80 MeV Cd ions showed good agreement with the distribution of measured leakage currents, as shown in Fig. 32.

X. SUMMARY AND CONCLUSION

MRED computes energy deposition in materials of arbitrary composition and structure by tabulating the energy lost through electronic excitation (electronic stopping) and atom-atom collisions (nuclear stopping) separately. For single event upsets and total ionizing dose effects, the key mechanism is electronic stopping. We have used MRED to study a variety of single

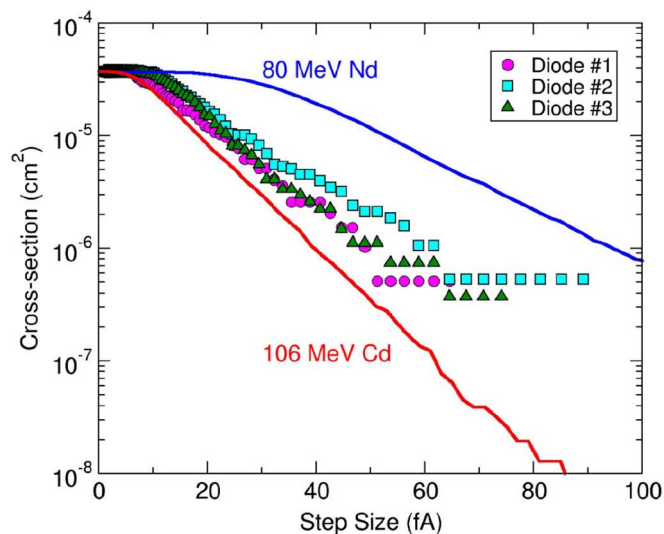


Fig. 32. Integral cross-section of fission fragment-induced discrete increases in diode leakage current compared to distributions of leakage current increases calculated from MRED (V9 G4.9.4) simulations of damage caused by 106 MeV Nd and 80 MeV Cd. (After [90]).

event upset mechanisms and on-orbit failure rates. Some of those studies were focused on understanding observed anomalous effects during experimental campaigns or on-orbit observations, e.g., single event upsets due to nuclear reactions produced by heavy ions and low energy protons. Other studies were predictive in nature. MRED was used to predict an observable prior to experimental verification, e.g., muon and electron induced SEU.

Similar to single event upset, electronic stopping is the key metric for total ionizing dose effects. We have demonstrated methods to use MRED to compute TID effects by studying dose enhancement effects when high-Z material consistent with new gate stacks are placed near oxides. MRED's ability to track nuclear stopping was used to study displacement damage effects. The rates of nonionizing energy loss were computed in LEDs and Si JFETs, and compared to experimental values to obtain insight into the resulting device degradation. MRED was also used to compute displacement damage distributions in HgCdTe focal plane arrays and Si JFETs. Taken together, these results demonstrate that MRED enables a broad range of validated simulation and analysis capabilities that facilitate the computation of energy deposition and transport in microelectronic materials and devices. The combination of MRED simulations and a targeted experimental test campaign can provide more accurate error rate calculations for a broad range of devices and integrated circuits in the space environment than was previously possible using traditional methods.

ACKNOWLEDGMENT

The authors wish to thank members of the Geant4 collaboration and in particular M. Asai, D. Wright, and T. Koi, Stanford Linear Accelerator Laboratory, for a most enjoyable and fruitful collaboration. A. Sierk and S. Mashnik, Los Alamos National Laboratory, have been of inestimable help in our effort to obtain and integrate the LANL codes LAQGSM and CEM03 into MRED. We especially thank F. Salvat, Facultat de Fisica, Universitat de Barcelona, Spain, for permission to use PENelope

2008 and Makoto Asai for his PENELOPE/Geant4 interface. The computing resources and system level support for this work were provided by the Advanced Computing Center for Research and Education (ACCRE) at Vanderbilt University. The authors also wish to thank Silvaco Inc. for supplying the TCAD tools used during this research.

REFERENCES

- [1] R. A. Reed *et al.*, “Anthology of the development of radiation transport tools as applied to single event effects,” *IEEE Trans. Nucl. Sci.*, vol. 60, no. 3, pp. 1876–1911, Jun. 2013.
- [2] P. Roche, G. Gasiot, J. L. Autran, D. Munteanu, R. A. Reed, and R. A. Weller, “Application of the TIARA radiation transport tool to single event effects simulation,” *IEEE Trans. Nucl. Sci.*, vol. 61, no. 3, pp. 1498–1500, Jun. 2014.
- [3] R. A. Weller, M. H. Mendenhall, R. A. Reed, R. D. Schrimpf, K. M. Warren, B. D. Sierawski, and L. W. Massengill, “Monte Carlo simulation of single event effects,” *IEEE Trans. Nucl. Sci.*, vol. 57, no. 4, pp. 1726–1746, Aug. 2010.
- [4] S. Agostinelli *et al.*, “GEANT4 - a simulation toolkit,” *Nucl. Instrum. Methods Phys. Res. A*, vol. 506, no. 3, pp. 250–303, 2003.
- [5] J. Allison *et al.*, “Geant4 developments and applications,” *IEEE Trans. Nucl. Sci.*, vol. 53, no. 1, pp. 270–278, Feb. 2006.
- [6] The Geant4 software [Online]. Available: <http://geant4.web.cern.ch/geant4/>
- [7] S. G. Mashnik, A. J. Sierk, K. K. Gudima, and M. I. Baznat, “CEM03 and LAQGSM03-new modeling tools for nuclear applications,” *J. Phys., Conf. Ser.*, vol. 41, no. 1, pp. 340–351, 2006.
- [8] S. G. Mashnik, K. K. Gudima, N. V. Mokhov, and R. E. Prael, LAQGSM3.03 upgrade and its validation [Online]. Available: <http://arxiv.org/abs/0709.1736>
- [9] S. G. Mashnik, K. K. Gudima, R. E. Prael, A. J. Sierk, M. I. Baznat, and N. V. Mokhov, CEM03.03 and LAQGSM03.03 event generators for the MCNP6, MCNPX, and MARS15 transport codes [Online]. Available: <http://arxiv.org/abs/0805.0751>
- [10] W. Shockley, “Problems related to p-n junctions in silicon,” *Solid-State Electron*, vol. 2, no. 1, pp. 35–67, 1961.
- [11] T. E. Oliphant, “Python for scientific computing,” *Comput. Sci. Eng.*, vol. 9, no. 3, pp. 10–20, May–Jun. 2007.
- [12] “Python programming language - official website,” [Online]. Available: <http://www.python.org>
- [13] D. M. Beazley, “SWIG: An easy to use tool for integrating scripting languages with C and C++,” in *Proc. 4th Annu. Tcl/Tk Workshop*, Berkeley, CA, USA, Jul. 10–13, 1996, pp. 129–39.
- [14] D. M. Beazley, “An extensible compiler for creating scriptable scientific software,” Computational Science-Iccs 2002 Pt II, Proc Lecture Notes in Computer Science P. Sloot, C. J. K. Tan, J. J. Dongarra, and A. G. Hoekstra, Eds., pp. 824–833, 2002.
- [15] T. L. Cottom, “Using SWIG to bind C++ to python,” *Comput. Sci. Eng.*, vol. 5, no. 2, pp. 88–97, 2003.
- [16] M. H. Mendenhall and R. A. Weller, “Algorithms for the rapid computation of classical cross sections for screened coulomb collisions,” *Nucl. Instrum. Methods Phys. Res. B*, vol. B58, no. 1, pp. 11–17, 1991.
- [17] M. H. Mendenhall and R. A. Weller, “An algorithm for ab initio computation of small-angle-multiple scattering angular distributions,” *Nucl. Instrum. Methods Phys. Res. B*, vol. B93, no. 1, pp. 5–10, 1994.
- [18] “Stopping of ions heavier than helium (Report 73),” J. the ICRU vol. 5, no. 1, pp. 1–253, 2005.
- [19] J. Baro, J. Sempau, J. M. Fernandez-Varea, and F. Salvat, “PENELOPE: An algorithm for Monte Carlo simulation of the penetration and energy loss of electrons and positrons in matter,” *Nucl. Instrum. Methods Phys. Res. B*, vol. B100, no. 1, pp. 31–46, 1995.
- [20] A. F. Bielajew and F. Salvat, “Improved electron transport mechanics in the PENELOPE Monte-Carlo model,” *Nucl. Instrum. Methods Phys. Res. B*, vol. 173, no. 3, pp. 332–343, 2001.
- [21] F. Salvat, J. Fernandez-Varea, and J. Sempau, “PENELOPE, a code system for Monte Carlo simulation of electron and photon transport (2nd edition),” in *Proc. OECD-NEA Workshop*, Issy-les-Moulineaux, France, 2003, vol. 241.
- [22] J. Sempau, J. M. Fernandez-Varea, E. Acosta, and F. Salvat, “Experimental benchmarks of the Monte Carlo code PENELOPE,” *Nucl. Instrum. Methods Phys. Res. B*, vol. 207, no. 2, pp. 107–123, Jun. 2003.
- [23] F. Salvat and J. M. Fernandez-Varea, “Overview of physical interaction models for photon and electron transport used in Monte Carlo codes,” *Metrologia*, vol. 46, no. 2, pp. S112–S138, 2009.
- [24] F. Salvat, J. M. Fernandez-Varea, and J. Sempau, “PENELOPE-2008: A code system for Monte Carlo simulation of electron and photon transport,” in *Proc. Workshop*, Barcelona, Spain, 2009, OECD Nuclear Energy Agency No. 6416.
- [25] M. H. Mendenhall and R. A. Weller, “A probability-conserving cross-section biasing mechanism for variance reduction in Monte Carlo particle transport calculations,” *Nucl. Instrum. Methods Phys. Res. A*, vol. 667, pp. 38–43, 2012.
- [26] A. S. Kobayashi, D. R. Ball, K. M. Warren, R. A. Reed, N. F. Haddad, M. H. Mendenhall, R. D. Schrimpf, and R. A. Weller, “The effect of metallization layers on single event susceptibility,” *IEEE Trans. Nucl. Sci.*, vol. 52, no. 6, pp. 2189–2193, Dec. 2005.
- [27] D. R. Ball, K. M. Warren, R. A. Weller, R. A. Reed, A. Kobayashi, J. A. Pellish, M. H. Mendenhall, C. L. Howe, L. W. Massengill, R. D. Schrimpf, and N. F. Haddad, “Simulating nuclear events in a TCAD model of a high-density SEU hardened SRAM technology,” *IEEE Trans. Nucl. Sci.*, vol. 53, no. 4, pp. 1794–1798, Aug. 2006.
- [28] R. Ecoffet, S. Duzellier, D. Falguere, L. Guibert, and C. Inguibert, “Low LET cross-section measurements using high energy carbon beam,” *IEEE Trans. Nucl. Sci.*, vol. 44, no. 6, pp. 2230–2236, Dec. 1997.
- [29] R. Koga, S. H. Crain, W. R. Crain, K. B. Crawford, and S. J. Hansel, “Comparative SEU sensitivities to relativistic heavy ions,” *IEEE Trans. Nucl. Sci.*, vol. 45, no. 6, pp. 2475–2482, Dec. 1998.
- [30] K. M. Warren, R. A. Weller, M. H. Mendenhall, R. A. Reed, D. R. Ball, C. L. Howe, B. D. Olson, M. L. Alles, L. W. Massengill, R. D. Schrimpf, N. F. Haddad, S. E. Doyle, D. McMorrow, J. S. Melinger, and W. T. Lotshaw, “The contribution of nuclear reactions to heavy ion single event upset cross-section measurements in a high-density SEU hardened SRAM,” *IEEE Trans. Nucl. Sci.*, vol. 52, no. 6, pp. 2125–2131, Dec. 2005.
- [31] N. A. Dodds, R. A. Reed, M. H. Mendenhall, R. A. Weller, M. A. Clemens, P. E. Dodd, M. R. Shaneyfelt, G. Vizelethy, J. R. Schwank, V. Ferlet-Cavrois, J. H. Adams, R. D. Schrimpf, and M. P. King, “Charge generation by secondary particles from nuclear reactions in BEOL materials,” *IEEE Trans. Nucl. Sci.*, vol. 56, no. 6, pp. 3172–3179, Dec. 2009.
- [32] W. Heinrich, “Calculation of LET-spectra of heavy cosmic ray nuclei at various absorber depths,” *Radiat. Eff.*, vol. 34, pp. 143–148, 1977.
- [33] P. E. Dodd, J. R. Schwank, M. R. Shaneyfelt, V. Ferlet-Cavrois, P. Paillet, J. Baggio, G. L. Hash, J. A. Felix, K. Hirose, and H. Saito, “Heavy ion energy effects in CMOS SRAMs,” *IEEE Trans. Nucl. Sci.*, vol. 54, no. 4, pp. 889–893, Aug. 2007.
- [34] C. L. Howe, R. A. Weller, R. A. Reed, M. H. Mendenhall, R. D. Schrimpf, K. M. Warren, D. R. Ball, L. W. Massengill, K. A. LaBel, J. W. Howard, Jr., and N. F. Haddad, “Role of heavy-ion nuclear reactions in determining on-orbit single event error rates,” *IEEE Trans. Nucl. Sci.*, vol. 52, no. 6, pp. 2182–2188, Dec. 2005.
- [35] R. A. Reed, R. A. Weller, M. H. Mendenhall, J. M. Lauenstein, K. M. Warren, J. A. Pellish, R. D. Schrimpf, B. D. Sierawski, L. W. Massengill, P. E. Dodd, M. R. Shaneyfelt, J. A. Felix, J. R. Schwank, N. F. Haddad, R. K. Lawrence, J. H. Bowman, and R. Conde, “Impact of ion energy and species on single event effects analysis,” *IEEE Trans. Nucl. Sci.*, vol. 54, no. 6, pp. 2312–2321, Dec. 2007.
- [36] P. J. McNulty, G. E. Farrell, R. C. Wyatt, P. L. Rothwell, R. C. Filz, and J. N. Bradford, “Upset phenomena induced by energetic protons and electrons,” *IEEE Trans. Nucl. Sci.*, vol. NS-27, no. 6, pp. 1516–1522, Dec. 1980.
- [37] W. L. Bendel and E. L. Petersen, “Proton upsets in orbit,” *IEEE Trans. Nucl. Sci.*, vol. 30, no. 6, pp. 4481–4485, Dec. 1983.
- [38] S. Gerardin, M. Bagatin, P. Rech, A. Cester, and A. Paccagnella, “Exploiting a low-energy accelerator to test commercial electronics with low-LET proton beams,” in *Proc. Radiation Effects in Components and Systems Workshop*, Athens, Greece, 2006.
- [39] K. P. Rodbell, D. F. Heidel, H. H. K. Tang, M. S. Gordon, P. Oldiges, and C. E. Murray, “Low-energy proton-induced single-event-upsets in 65 nm node, silicon-on-insulator, latches and memory cells,” *IEEE Trans. Nucl. Sci.*, vol. 54, no. 6, pp. 2474–2479, Dec. 2007.
- [40] D. F. Heidel, K. P. Rodbell, P. Oldiges, M. S. Gordon, H. H. K. Tang, E. H. Cannon, and C. Plettner, “Single-event-upset critical charge measurements and modeling of 65 nm silicon-on-insulator latches and memory cells,” *IEEE Trans. Nucl. Sci.*, vol. 53, no. 6, pp. 3512–3517, Dec. 2006.

- [41] B. D. Sierawski, J. A. Pellish, R. A. Reed, R. D. Schrimpf, K. M. Warren, R. A. Weller, M. H. Mendenhall, J. D. Black, A. D. Tipton, M. A. Xapsos, R. C. Baumann, D. Xiaowei, M. J. Campola, M. R. Friendlich, H. S. Kim, A. M. Phan, and C. M. Seidleck, "Impact of low-energy proton induced upsets on test methods and rate predictions," *IEEE Trans. Nucl. Sci.*, vol. 56, no. 6, pp. 3085–3092, Dec. 2009.
- [42] D. F. Heidel, P. W. Marshall, J. A. Pellish, K. P. Rodbell, K. A. LaBel, J. R. Schwank, S. E. Rauch, M. C. Hakey, M. D. Berg, C. M. Castaneda, P. E. Dodd, M. R. Friendlich, A. D. Phan, C. M. Seidleck, M. R. Shaneyfelt, and M. A. Xapsos, "Single-event upsets and multiple-bit upsets on a 45 nm SOI SRAM," *IEEE Trans. Nucl. Sci.*, vol. 56, no. 6, pp. 3499–3504, Dec. 2009.
- [43] J. R. Schwank, M. R. Shaneyfelt, V. Ferlet-Cavrois, P. E. Dodd, E. W. Blackmore, J. A. Pellish, K. P. Rodbell, D. F. Heidel, P. W. Marshall, K. A. LaBel, P. M. Gouker, N. Tam, R. Wong, W. Shi-Jie, R. A. Reed, S. M. Dalton, and S. E. Swanson, "Hardness assurance testing for proton direct ionization effects," *IEEE Trans. Nucl. Sci.*, vol. 59, no. 4, pp. 1197–1202, Aug. 2012.
- [44] C. Weulersse, F. Miller, D. Alexandrescu, E. Schaefer, and R. Gaillard, "Assessment and comparison of the low energy proton sensitivity in 65 nm to 28 nm SRAM devices," in *Proc. 12th Eur. Conf. Radiation and Effects on Components and Systems*, Sevilla, Spain, 2011, pp. 291–296.
- [45] E. H. Cannon, M. Cabanas-Holmen, J. Wert, T. Amort, R. Brees, J. Koehn, B. Meaker, and E. Normand, "Heavy ion, high-energy, and low-energy proton SEE sensitivity of 90-nm RHBD SRAMs," *IEEE Trans. Nucl. Sci.*, vol. 57, no. 6, pp. 3493–3499, Dec. 2010.
- [46] N. F. Haddad, A. T. Kelly, R. K. Lawrence, L. Bin, J. C. Rodgers, J. F. Ross, K. M. Warren, R. A. Weller, M. H. Mendenhall, and R. A. Reed, "Incremental enhancement of SEU hardened 90 nm CMOS memory cell," *IEEE Trans. Nucl. Sci.*, vol. 58, no. 3, pp. 975–980, Jun. 2011.
- [47] N. A. Dodds, J. R. Schwank, M. R. Shaneyfelt, P. E. Dodd, B. L. Doyle, M. Trinczek, E. W. Blackmore, K. P. Rodbell, M. S. Gordon, R. A. Reed, J. A. Pellish, K. A. LaBel, P. W. Marshall, S. E. Swanson, G. Vizkelethy, S. Van Deusen, F. W. Sexton, and M. J. Martinez, "Hardness assurance for proton direct ionization-induced SEEs using a high-energy proton beam," *IEEE Trans. Nucl. Sci.*, vol. 61, no. 6, pp. 2904–2914, Dec. 2014.
- [48] B. D. Sierawski, B. Bhuvu, R. Reed, K. Ishida, N. Tam, A. Hillier, B. Narasimham, M. Trinczek, E. Blackmore, W. Shi-Jie, and R. Wong, "Bias dependence of muon-induced single event upsets in 28 nm static random access memories," in *Proc. IEEE Int. Reliability Physics Symp.*, Hilton Waikoloa Village Waikoloa, HI, USA, 2014, pp. 2B.2.1–2B.2.5.
- [49] K. M. Warren, B. D. Sierawski, R. A. Weller, R. A. Reed, M. H. Mendenhall, J. A. Pellish, R. D. Schrimpf, L. W. Massengill, M. E. Porter, and J. D. Wilkinson, "Predicting thermal neutron-induced soft errors in static memories using TCAD and physics-based Monte Carlo simulation tools," *IEEE Electron Device Lett.*, vol. 28, no. 2, pp. 180–182, 2007.
- [50] K. M. Warren, R. A. Weller, B. D. Sierawski, R. A. Reed, M. H. Mendenhall, R. D. Schrimpf, L. W. Massengill, M. E. Porter, J. D. Wilkinson, K. A. LaBel, and J. H. Adams, "Application of RADSAFE to model the single event upset response of a 0.25 μm CMOS SRAM," *IEEE Trans. Nucl. Sci.*, vol. 54, no. 4, pp. 898–903, Aug. 2007.
- [51] E. Normand, "Single event upset at ground level," *IEEE Trans. Nucl. Sci.*, vol. 43, no. 6, pp. 2742–2750, Dec. 1996.
- [52] B. D. Sierawski, M. H. Mendenhall, R. A. Reed, M. A. Clemens, R. A. Weller, R. D. Schrimpf, E. W. Blackmore, M. Trinczek, B. Hitti, J. A. Pellish, R. C. Baumann, W. Shi-Jie, R. Wong, and N. Tam, "Muon-induced single event upsets in deep-submicron technology," *IEEE Trans. Nucl. Sci.*, vol. 57, no. 6, pp. 3273–3278, Dec. 2010.
- [53] G. M. Marshall, "Muon beams and facilities at TRIUMF," *Z. Phys. C, Part. Fields*, vol. 56, no. 1, pp. S226–S231, 1992.
- [54] T. Matsuzaki, K. Ishida, K. Nagamine, I. Watanabe, G. H. Eaton, and W. G. Williams, "The RIKEN-RAL pulsed muon facility," *Nucl. Instrum. Methods Phys. Res. A*, vol. 465, no. 2–3, pp. 365–383, 2001.
- [55] S. Bourdarie and M. Xapsos, "The near-Earth space radiation environment," *IEEE Trans. Nucl. Sci.*, vol. 55, no. 4, pp. 1810–1832, Aug. 2008.
- [56] M. A. Xapsos, P. M. O'Neill, and T. P. O'Brien, "Near-Earth space radiation models," *IEEE Trans. Nucl. Sci.*, vol. 60, no. 3, pp. 1691–1705, Jun. 2013.
- [57] R. A. Weller, A. L. Sternberg, L. W. Massengill, R. D. Schrimpf, and D. M. Fleetwood, "Evaluating average and atypical response in radiation effects simulations," *IEEE Trans. Nucl. Sci.*, vol. 50, no. 6, pp. 2265–2271, Dec. 2003.
- [58] M. Raine, G. Hubert, M. Gaillardin, L. Artola, P. Paillet, S. Girard, J. E. Sauvestre, and A. Bournel, "Impact of the radial ionization profile on SEE prediction for SOI transistors and SRAMs beyond the 32-nm technological node," *IEEE Trans. Nucl. Sci.*, vol. 58, no. 3, pp. 840–847, Jun. 2011.
- [59] M. P. King, R. A. Reed, R. A. Weller, M. H. Mendenhall, R. D. Schrimpf, M. L. Alles, E. C. Auden, S. E. Armstrong, and M. Asai, "The impact of delta-rays on single-event upsets in highly scaled SOI SRAMs," *IEEE Trans. Nucl. Sci.*, vol. 57, no. 6, pp. 3169–3175, Dec. 2010.
- [60] M. P. King, R. A. Reed, R. A. Weller, M. H. Mendenhall, R. D. Schrimpf, N. D. Pate, E. A. Auden, and S. L. Weeden-Wright, "Radial characteristics of heavy-ion track structure and implications of delta-ray events for microelectronics," *Appl. Phys. Lett.*, vol. 101, no. 5, p. 053509, 2012.
- [61] M. P. King *et al.*, "Electron-induced single-event upsets in static random access memory," *IEEE Trans. Nucl. Sci.*, vol. 60, no. 6, pp. 4122–4129, Dec. 2013.
- [62] A. Samaras, P. Pourrouquet, N. Sukhaseum, L. Gouyet, B. Vandevelde, N. Chattry, R. Ecoffet, F. Bezerra, and E. Lorfevre, "Experimental characterization and simulation of electron-induced SEU in 45-nm CMOS technology," *IEEE Trans. Nucl. Sci.*, vol. 61, no. 6, pp. 3055–3060, Dec. 2014.
- [63] M. G. Buehler and B. R. Blaes, "Alpha-particle sensitive test SRAMs," *IEEE Trans. Nucl. Sci.*, vol. 37, no. 6, pp. 1849–1854, Dec. 1990.
- [64] J. Barak, J. Levinson, A. Akkerman, E. Adler, A. Zentner, D. David, Y. Lifshitz, M. Hass, B. E. Fischer, M. Schlögl, M. Victoria, and W. Haddad, "Scaling of SEU mapping and cross section, and proton induced SEU at reduced supply voltage," *IEEE Trans. Nucl. Sci.*, vol. 46, no. 6, pp. 1342–1353, Dec. 1999.
- [65] J. Barak, A. Haran, E. Adler, M. Azoulay, J. Levinson, A. Zentner, D. David, B. E. Fischer, M. Heiss, and D. Betel, "Use of light-ion-induced SEU in devices under reduced bias to evaluate their SEU cross section," *IEEE Trans. Nucl. Sci.*, vol. 51, no. 6, pp. 3486–3493, Dec. 2004.
- [66] C. M. Dozier and D. B. Brown, "The use of low energy x-rays for device testing - A comparison with Co-60 radiation," *IEEE Trans. Nucl. Sci.*, vol. NS-30, no. 6, pp. 4382–4387, Dec. 1983.
- [67] I. Jun, H. B. Garrett, and R. W. Evans, "High-energy trapped particle environments at Jupiter: An update," *IEEE Trans. Nucl. Sci.*, vol. 52, no. 6, pp. 2281–2286, Dec. 2005.
- [68] A. D. Tipton, J. A. Pellish, R. A. Reed, R. D. Schrimpf, R. A. Weller, M. H. Mendenhall, B. Sierawski, A. K. Sutton, R. M. Diestelhorst, G. Espinel, J. D. Cressler, P. W. Marshall, and G. Vizkelethy, "Multiple-bit upset in 130 nm CMOS technology," *IEEE Trans. Nucl. Sci.*, vol. 53, no. 6, pp. 3259–3264, Dec. 2006.
- [69] L. W. Massengill, "Cosmic and terrestrial single-event radiation effects in dynamic random access memories," *IEEE Trans. Nucl. Sci.*, vol. 43, no. 2, pp. 576–593, Apr. 1996.
- [70] N. Seifert, P. Slankard, M. Kirsch, B. Narasimham, V. Zia, C. Brookreson, A. Vo, S. Mitra, B. Gill, and J. Maiz, "Radiation-induced soft error rates of advanced CMOS bulk devices," in *Proc. 44th Annu. IEEE Int. Reliability Physics Symp.*, San Jose, CA, USA, 2006, pp. 217–225.
- [71] R. A. Reed, P. W. Marshall, H. S. Kim, P. J. McNulty, B. Fodness, T. A. Jordan, R. Reedy, C. Tabbert, M. S. T. Liu, W. Heikkilä, S. Buchner, R. Ladbury, and K. A. LaBel, "Evidence for angular effects in proton-induced single-event upsets," *IEEE Trans. Nucl. Sci.*, vol. 49, no. 6, pp. 3038–3044, Dec. 2002.
- [72] S. Buchner, A. Campbell, R. Reed, B. Fodness, and S. Kuboyama, "Angular dependence of multiple-bit upsets induced by protons in a 16 mbit DRAM," *IEEE Trans. Nucl. Sci.*, vol. 51, no. 6, pp. 3270–3277, Dec. 2004.
- [73] J. Maiz, S. Hareland, K. Zhang, and P. Armstrong, "Characterization of multi-bit soft error events in advanced SRAMs," in *Proc. IEEE Int. Electron Devices Meeting*, Washington, DC, USA, 2003, pp. 21.4.1–21.4.4.
- [74] H. Quinn, P. Graham, J. Krone, M. Caffrey, and S. Rezgui, "Radiation-induced multi-bit upsets in SRAM-based FPGAs," *IEEE Trans. Nucl. Sci.*, vol. 52, no. 6, pp. 2455–2461, Dec. 2005.
- [75] D. Radaelli, H. Puchner, W. Skip, and S. Daniel, "Investigation of multi-bit upsets in a 150 nm technology SRAM device," *IEEE Trans. Nucl. Sci.*, vol. 52, no. 6, pp. 2433–2437, Dec. 2005.
- [76] Y. Tosaka, H. Ehara, M. Igeta, T. Uemura, H. Oka, N. Matsuoka, and K. Hatanaka, "Comprehensive study of soft errors in advanced CMOS circuits with 90/130 nm technology," in *Proc. IEEE Int. Elect. Dev. Meeting*, San Francisco, CA, USA, 2004, pp. 941–944.

- [77] F. Wrobel, J. M. Palau, M. C. Calvet, O. Bersillon, and H. Duarte, "Simulation of nucleon-induced nuclear reactions in a simplified SRAM structure: Scaling effects on SEU and MBU cross sections," *IEEE Trans. Nucl. Sci.*, vol. 48, no. 6, pp. 1946–1952, Dec. 2001.
- [78] A. D. Tipton, J. A. Pellish, J. M. Hutson, R. Baumann, X. Deng, A. Marshall, M. A. Xapsos, H. S. Kim, M. R. Friendlich, M. J. Campola, C. M. Seidleck, K. A. LaBel, M. H. Mendenhall, R. A. Reed, R. D. Schrimpf, R. A. Weller, and J. D. Black, "Device-orientation effects on multiple-bit upset in 65 nm SRAMs," *IEEE Trans. Nucl. Sci.*, vol. 55, no. 6, pp. 2880–2885, Dec. 2008.
- [79] A. D. Tipton, Z. Xiaowei, W. Haixiao, J. A. Pellish, P. R. Fleming, R. D. Schrimpf, R. A. Reed, R. A. Weller, and M. Mendenhall, "Increased rate of multiple-bit upset from neutrons at large angles of incidence," *IEEE Trans. Device Mater. Rel.*, vol. 8, no. 3, pp. 565–570, 2008.
- [80] A. Dasgupta, D. M. Fleetwood, R. A. Reed, R. A. Weller, M. H. Mendenhall, and B. D. Sierawski, "Dose enhancement and reduction in SiO₂ and high-k MOS insulators," *IEEE Trans. Nucl. Sci.*, vol. 57, no. 6, pp. 3463–3469, Dec. 2010.
- [81] D. M. Fleetwood, D. E. Beutler, L. J. Lorence, D. B. Brown, B. L. Draper, L. C. Riewe, H. B. Rosenstock, and D. P. Knott, "Comparison of enhanced device response and predicted X-ray dose enhancement effects on MOS oxides," *IEEE Trans. Nucl. Sci.*, vol. 35, no. 6, pp. 1265–1271, Dec. 1988.
- [82] D. E. Beutler, D. M. Fleetwood, W. Beezhold, D. Knott, L. J. Lorence, and B. L. Draper, "Variations in semiconductor device response in a medium-energy x-ray dose-enhancing environment," *IEEE Trans. Nucl. Sci.*, vol. NS-34, no. 6, pp. 1544–1550, Dec. 1987.
- [83] C. M. Dozier and D. B. Brown, "Effect of photon energy on the response of MOS devices," *IEEE Trans. Nucl. Sci.*, vol. NS-28, no. 6, pp. 4137–4141, Dec. 1981.
- [84] D. B. Brown, "Photoelectron effects on the dose deposited in MOS devices by low energy X-ray sources," *IEEE Trans. Nucl. Sci.*, vol. NS-27, no. 6, pp. 1465–1468, Dec. 1980.
- [85] J. R. Schwank, M. R. Shaneyfelt, D. M. Fleetwood, J. A. Felix, P. E. Dodd, P. Paillet, and V. Ferlet-Cavrois, "Radiation effects in MOS oxides," *IEEE Trans. Nucl. Sci.*, vol. 55, no. 4, pp. 1833–1853, Aug. 2008.
- [86] A. Dasgupta, D. M. Fleetwood, R. A. Reed, R. A. Weller, and M. H. Mendenhall, "Effects of metal gates and back-end-of-line materials on x-ray dose in HfO₂ gate oxide," *IEEE Trans. Nucl. Sci.*, vol. 58, no. 6, pp. 3139–3144, Dec. 2011.
- [87] S. K. Dixit, X. J. Zhou, R. D. Schrimpf, D. M. Fleetwood, S. T. Pantelides, R. Choi, G. Bersuker, and L. C. Feldman, "Radiation induced charge trapping in ultrathin HfO₂-based MOSFETs," *IEEE Trans. Nucl. Sci.*, vol. 54, no. 6, pp. 1883–1890, Dec. 2007.
- [88] J. R. Srour and J. W. Palko, "Displacement damage effects in irradiated semiconductor devices," *IEEE Trans. Nucl. Sci.*, vol. 60, no. 3, pp. 1740–1766, Jun. 2013.
- [89] R. A. Weller, M. H. Mendenhall, and D. M. Fleetwood, "A screened coulomb scattering module for displacement damage computations in Geant4," *IEEE Trans. Nucl. Sci.*, vol. 51, no. 6, pp. 3669–3678, Dec. 2004.
- [90] E. C. Auden, R. A. Weller, M. H. Mendenhall, R. A. Reed, R. D. Schrimpf, N. C. Hooten, and M. P. King, "Single particle displacement damage in silicon," *IEEE Trans. Nucl. Sci.*, vol. 59, no. 6, pp. 3054–3061, Dec. 2012.
- [91] C. J. Marshall, P. W. Marshall, C. L. Howe, R. A. Reed, R. A. Weller, M. Mendenhall, A. Waczynski, R. Ladbury, and T. M. Jordan, "Comparison of measured dark current distributions with calculated damage energy distributions in HgCdTe," *IEEE Trans. Nucl. Sci.*, vol. 54, no. 4, pp. 1097–1103, Aug. 2007.
- [92] E. C. Auden, R. A. Weller, R. D. Schrimpf, M. H. Mendenhall, R. A. Reed, N. C. Hooten, W. G. Bennett, and M. P. King, "Effects of high electric fields on the magnitudes of current steps produced by single particle displacement damage," *IEEE Trans. Nucl. Sci.*, vol. 60, no. 6, pp. 4094–4102, Dec. 2013.
- [93] J. Lindhard, V. Nielsen, M. Scharff, and P. V. Thomsen, "Integral equations governing radiation effects (notes on atomic collisions, III)," *K. Dan. Vidensk. Selsk., Mat.-Fys. Medd.*, vol. 33, no. 10, pp. 1–41, 1963.
- [94] G. P. Summers, E. A. Burke, P. Shapiro, S. R. Messenger, and R. J. Walters, "Damage correlations in semiconductors exposed to gamma, electron and proton radiations," *IEEE Trans. Nucl. Sci.*, vol. 40, no. 6, pp. 1372–1379, Dec. 1993.
- [95] S. R. Messenger, E. A. Burke, G. P. Summers, M. A. Xapsos, R. J. Walters, E. M. Jackson, and B. D. Weaver, "Nonionizing energy loss (NIEL) for heavy ions," *IEEE Trans. Nucl. Sci.*, vol. 46, no. 6, pp. 1595–1602, Dec. 1999.
- [96] E. A. Burke, C. J. Dale, A. B. Campbell, G. P. Summers, W. J. Stapor, M. A. Xapsos, T. Palmer, and R. Zuleeg, "Energy dependence of proton-induced displacement damage in gallium arsenide," *IEEE Trans. Nucl. Sci.*, vol. NS-34, no. 6, pp. 1220–1227, Dec. 1987.
- [97] I. Jun, M. A. Xapsos, S. R. Messenger, E. A. Burke, R. J. Walters, G. P. Summers, and T. Jordan, "Proton nonionizing energy loss (NIEL) for device applications," *IEEE Trans. Nucl. Sci.*, vol. 50, no. 6, pp. 1924–1928, Dec. 2003.
- [98] A. L. Barry, A. J. Houdayer, P. F. Hinrichsen, W. G. Letourneau, and J. Vincent, "The energy dependence of lifetime damage constants in GaAs LEDs for 1-500 MeV protons," *IEEE Trans. Nucl. Sci.*, vol. 42, no. 6, pp. 2104–2107, Dec. 1995.
- [99] C. J. Marshall and P. W. Marshall, "Proton effects and test issues for satellite designers: Displacement effects," in *Proc. IEEE Nuclear and Space Radiation Effects Conf. Short Course*, Norfolk, VA, USA, 1999, Section IVB.
- [100] MCNPX User's Manual (Version 2.4.0) LA-CP-02-408, L. S. Waters, Ed., Los Alamos National Laboratory, USA, 2002.
- [101] W. Shockley and W. T. Read, Jr., "Statistics of the recombinations of holes and electrons," *Phys. Rev.*, vol. 87, pp. 835–842, 1952.